Reuse of Hybrid Car Power Systems

by

Nicholas Kirkby

Submitted to the
Department of Mechanical Engineering
in Partial Fulfillment of the Requirements for the Degree of

Bachelor of Science in Mechanical Engineering

at the

Massachusetts Institute of Technology

June 2015

Signature of Author: Signature redacted
Department of Mechanical Engineering
April 14, 2015

Certified by: Signature redacted
James L. Kirtley Jr.
Professor of Electrical Engineering
Thesis Supervisor

Accepted by: Signature redacted
Anette Hosoi
Professor of Mechanical Engineering
Undergraduate Officer

Reuse of Hybrid Car Power Systems

by

Nicholas Kirkby

Submitted to the Department of Mechanical Engineering
on April 14, 2015 in Partial Fulfillment of the
Requirements for the Degree of

Bachelor of Science in Mechanical Engineering

ABSTRACT

Used hybrid car power systems are inexpensive and capable of tens of kilowatts of power throughput. This paper documents a process for using the second generation Toyota Prius inverter module to drive a three phase permanent magnet synchronous motor/generator from Ford hybrid vehicle. A lightweight housing and a rotor position sensor for the motor/generator are constructed to allow it to be used outside of the original bulky transaxle. Field oriented control is implemented on a microcontroller which interfaces with the motor/generator and the Prius inverter module. The motor, inverter, and controller are installed on a demonstration vehicle for the purpose of load testing.

Thesis Supervisor: James L. Kirtley Jr.
Tile: Professor of Electrical Engineering

Table of Contents

Motivation

The purpose of an undergraduate thesis is to learn some things and write about them. This project is the result of a simple desire to make a hybrid car motor spin.

It is exciting that power electronic systems are becoming increasingly reliable, efficient, and abundant through the growth of the hybrid vehicle industry. Even more exciting is that these components are available as inexpensive used car parts.

Scope

The work documented here sequentially covers the following four areas:

- Design and fabrication of a housing and rotor position detection system for a hybrid car motor/generator
- Using a second generation Prius inverter module to drive the motor/generator
- Implementation of field oriented control on a microprocessor
- Combination of the above subsystems on a demonstration vehicle for the purpose of load testing

Background

As shown in figure 1, the number of hybrid cars sold in the United States has been rising rapidly since approximately 2004. The majority of these cars are produced by automakers Toyota, Honda, and Ford. They contain electric motor/generators which are very similar in both appearance and functionality. This is because the hybrid transaxles of many popular cars are, or were originally designed by Aisin AW Co. LTD of Japan. Aisin AW Co. LTD is a division of the Aisin Seiki Corporation, specializing in the manufacture of automatic transmissions. With many mainstream hybrid cars now nearly a decade old, their parts are easy to find and inexpensive to purchase.

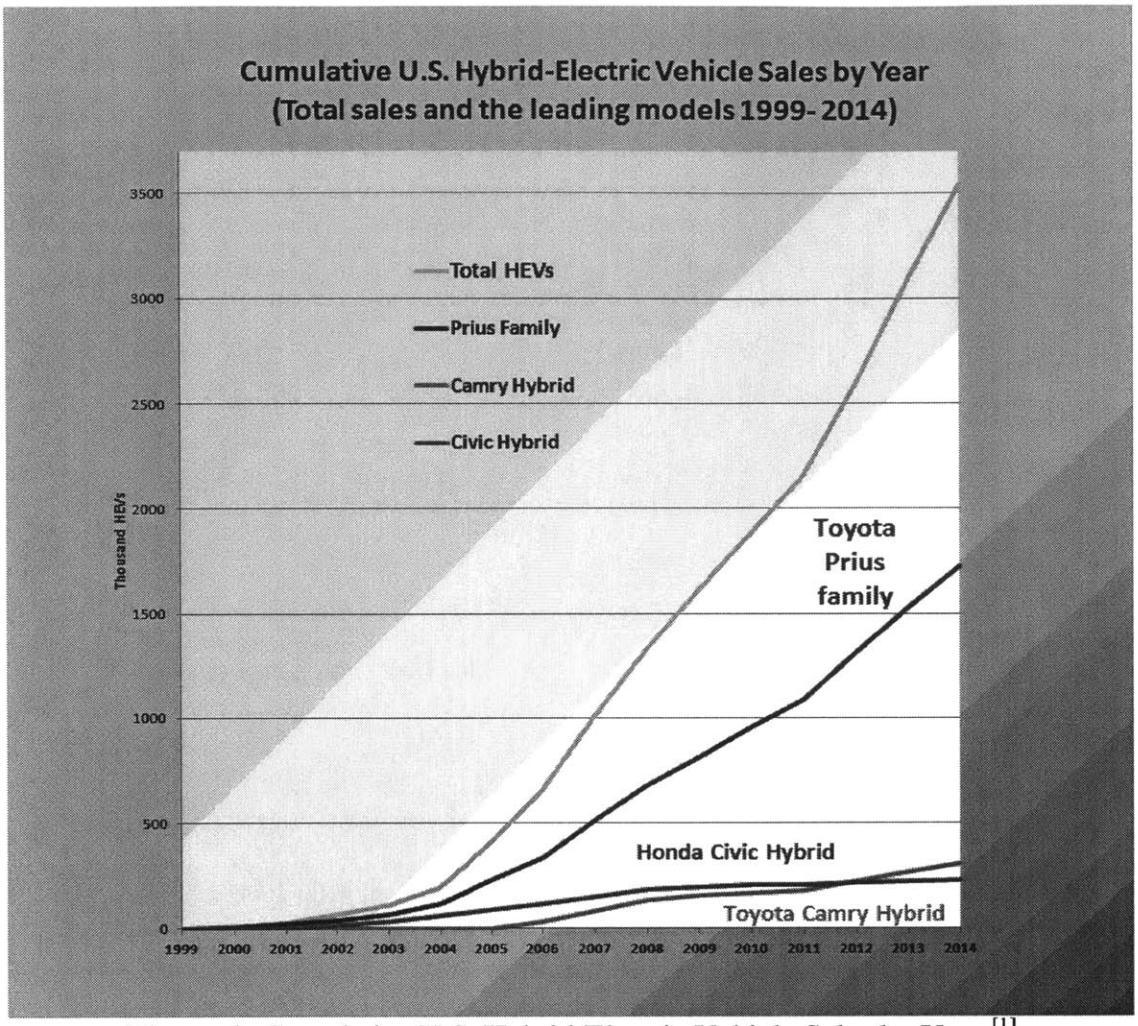

Figure 1: Cumulative U.S. Hybrid-Electric Vehicle Sales by Year [1]

Motor/Generators in Hybrid Vehicles

Whether an electric machine is a motor or a generator depends on the direction that energy takes through the machine. Generators convert torque and speed to current and voltage. Motors do the reverse, converting current and voltage to torque and speed.

A pair of motor/generators (figures 2 and 3) was left by MIT electric vehicle team when they converted a 2010 Mercury Milan Hybrid to be fully electric, replacing the hybrid transaxle and engine with a single SatCon induction motor. [2] The Mercury Milan Hybrid was not produced in such great quantities as the Prius, and as a result, its parts are more expensive on the surplus market.

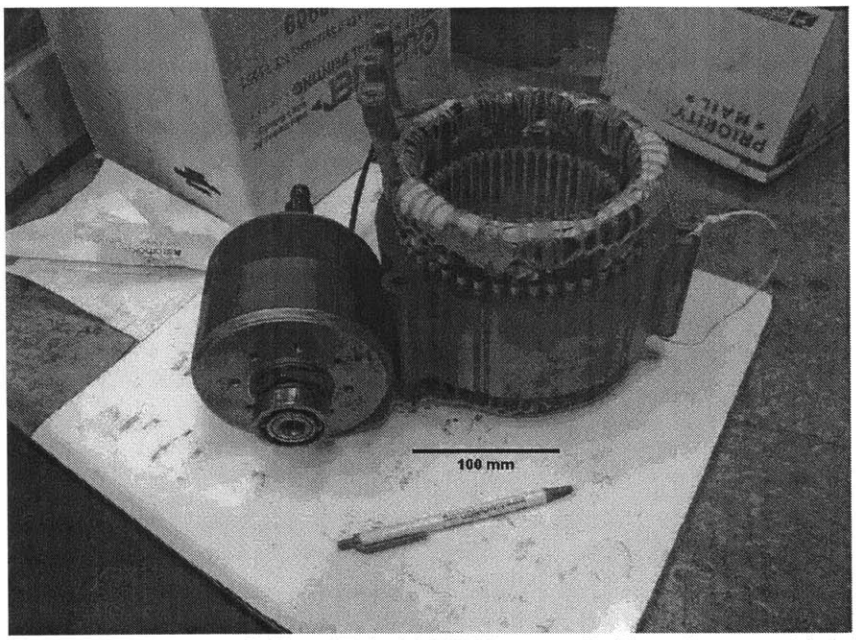

Figure 2: Mercury Milan Hybrid MG1 rotor (left) and stator (right)

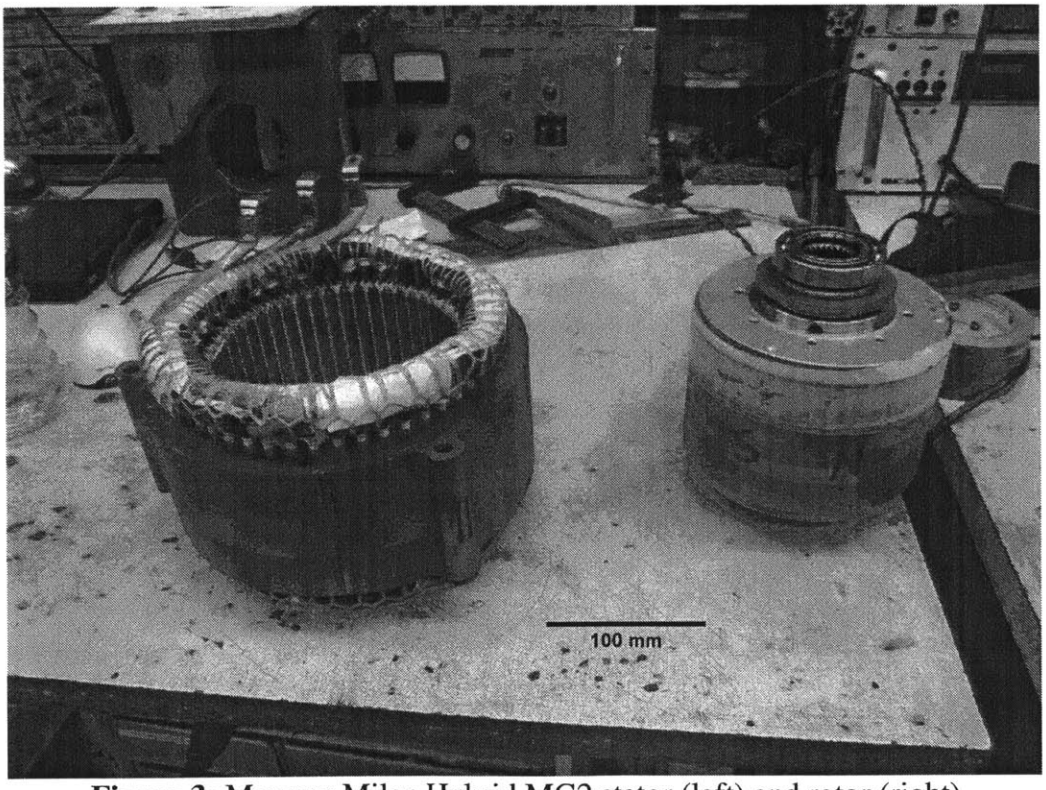

Figure 3: Mercury Milan Hybrid MG2 stator (left) and rotor (right)

Interior Permanent Magnet (IPM) Motor/Generator

An IPM machine typically has a laminated rotor with magnets buried within. Figure 4 shows a rotor punching from the 2004 Toyota Prius motor. The vee shaped slots hold permanent magnets which are magnetized radially outwards. This rotor has eight poles.

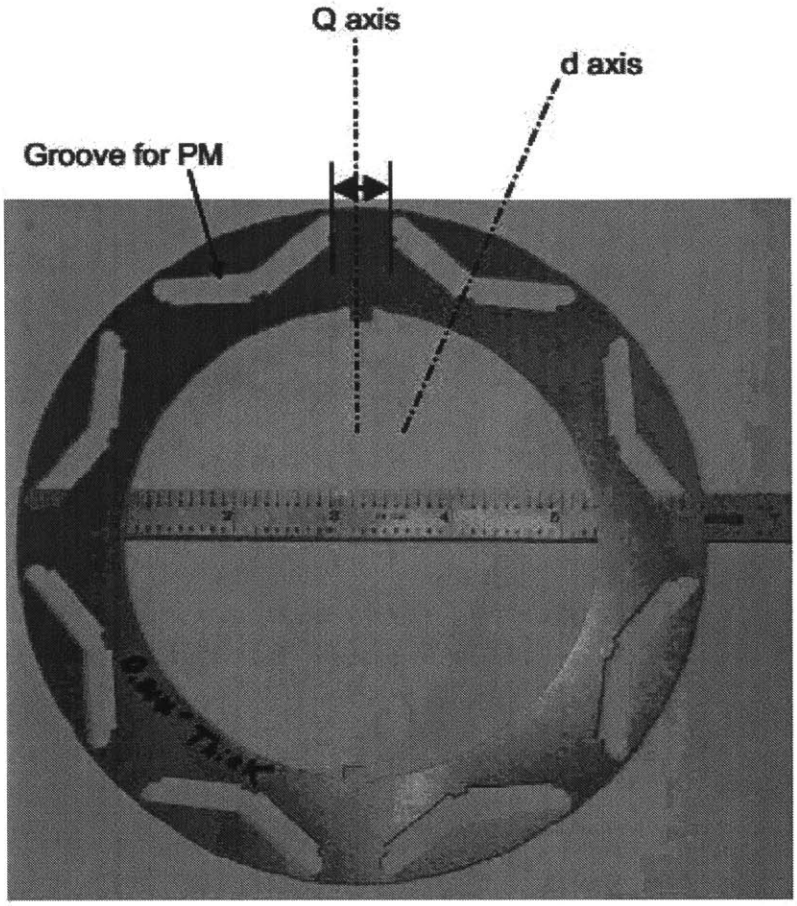

Figure 4: 2004 Prius rotor punching [3, p. 10]

The Mercury Milan Hybrid MG1 rotor is shown in detail in figure 5. The lamination stack is compressed between two cast and machined aluminum endplates. A nut is used to apply and retain compression. This seems to be a common manufacturing technique for this type of motor. Also notable is the rotor of the variable reluctance resolver (VRR). This lobed stack of steel laminations on the rotor is excited by a stationary set of windings. Depending on its rotational position, the amount of flux travelling through it changes. These changes are detected by another set of windings in the VRR stator and are processed to calculate rotor position. Figure 6 shows a VRR with a two pole pair rotor made by Cumatix.

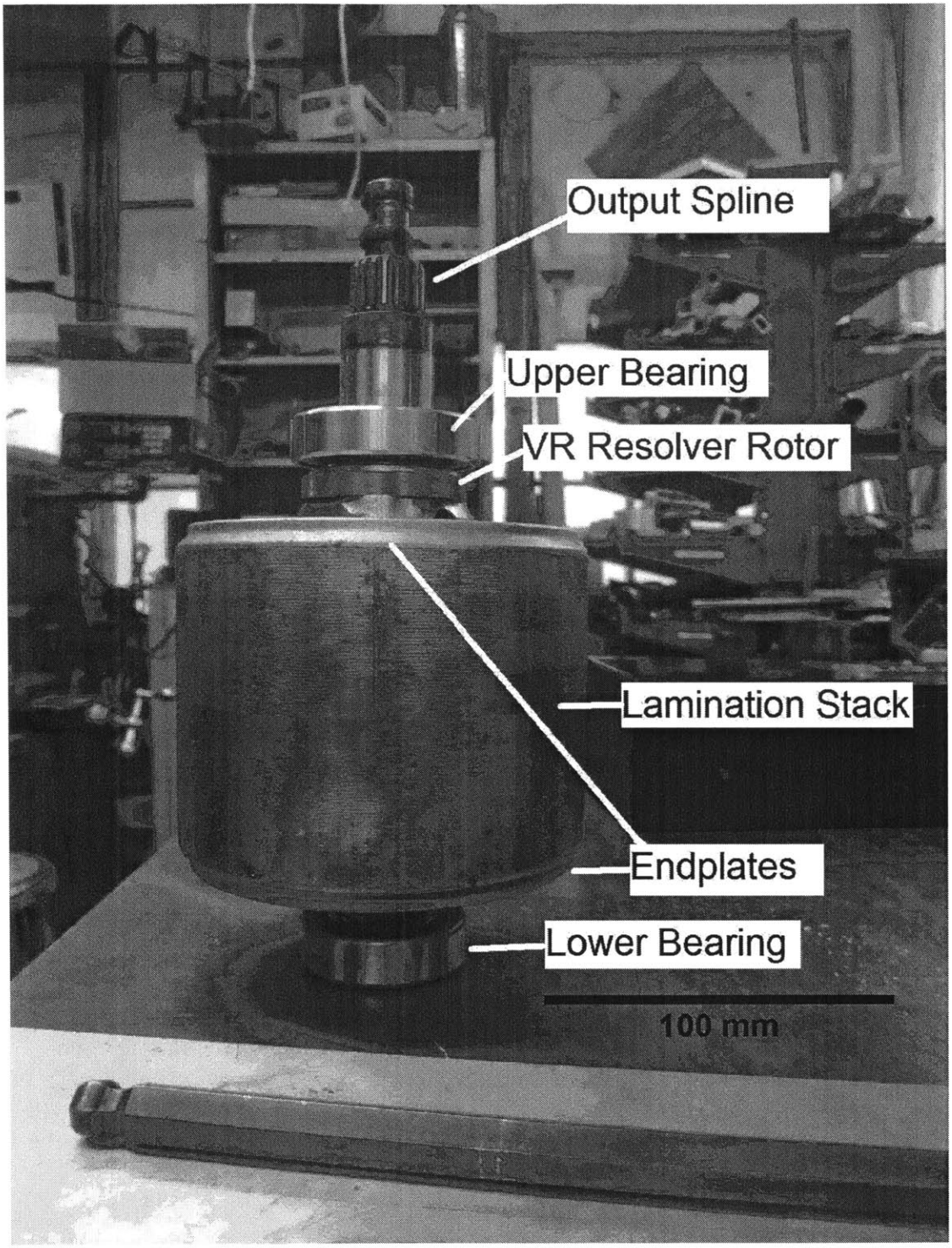

Figure 5: Annotated Mercury Milan MG1 rotor

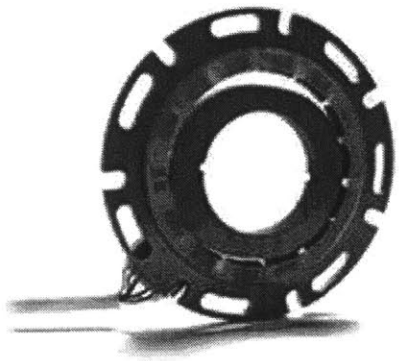

Figure 6: Variable reluctance resolver (VRR) sold by Cumatix for hybrid drivetrain applications[1]

Motor Housing

The rotors and stators as received were loose with no fixture for constraining them with respect to one another. A fixture is necessary to maintain a gap between rotor and stator so that the rotor may spin freely. In this case, the gap is a millimeter or less.

Typical Hybrid Transaxle Motor Housing

Figure <> shows a partly disassembled Prius transaxle. It is a large aluminum casting in which key mating surfaces such as bearing bores and the stator cavity have been CNC machined. These manufacturing methods are typical of hybrid vehicle transaxles.

[1] http://www.cumatix.com/en/sensors/vr-resolvers/

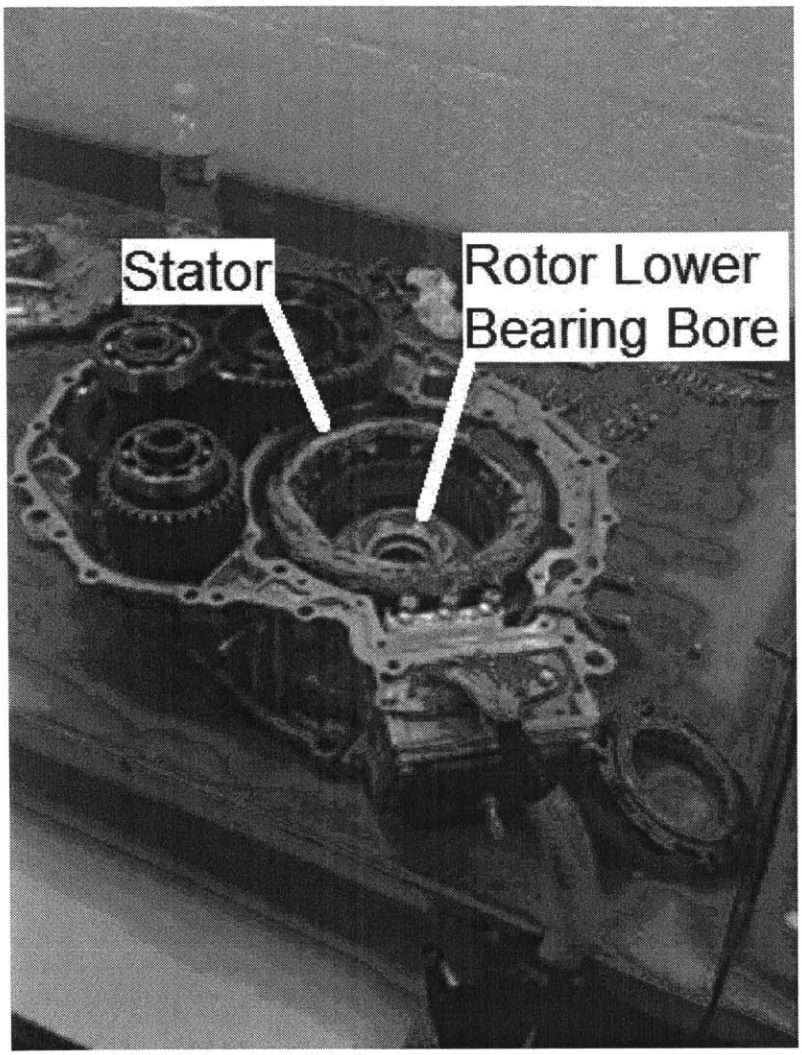

Figure 7: Prius transaxle showing highly integrated stator and gear reduction. (http://www.vibratesoftware.com/)

Design of Custom Housings

Separate housings were made for both MG1 and MG2. The housing for MG2 was made first. The process was then revised for the MG1 housing to improve ease of manufacture, constraint, and mechanical robustness. Only the revised process for MG1 is described here. Further details on the MG2 housing can be found on the author's website.[2]

[2] http://nkirkby.scripts.mit.edu/nk/

First, dimensionally accurate CAD models of the rotor and stator were made.

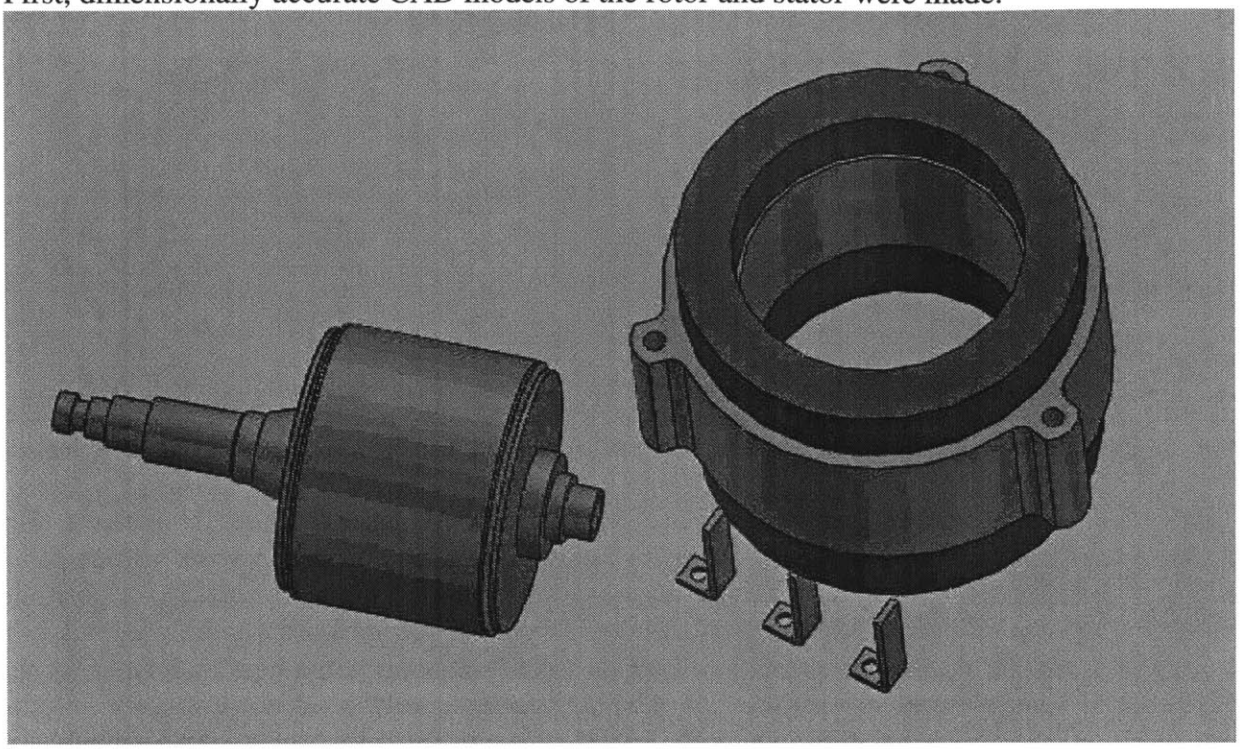

Figure 8: Models of rotor (left) and stator (right)

Next, a housing was designed. The table below lists the functional requirements that drove the design.

Functional Requirement	Acceptable Quantity	Measured Quantity
Holds rotor concentric with stator	Concentricity to within 0.1 mm	0.05 mm
Stiff enough to prevent rotor from touching stator during shock loading	Less than 0.5 mm deflection at endcap under 100 Kg loading	0.3 mm @ 100 Kg
Repeatable removal and realignment of back plate	Rotor should not rub after removing and replacing the back plate	Rotor does not rub after removal and replacement of back plate

Table 1: Functional Requirements for MG1 housing design

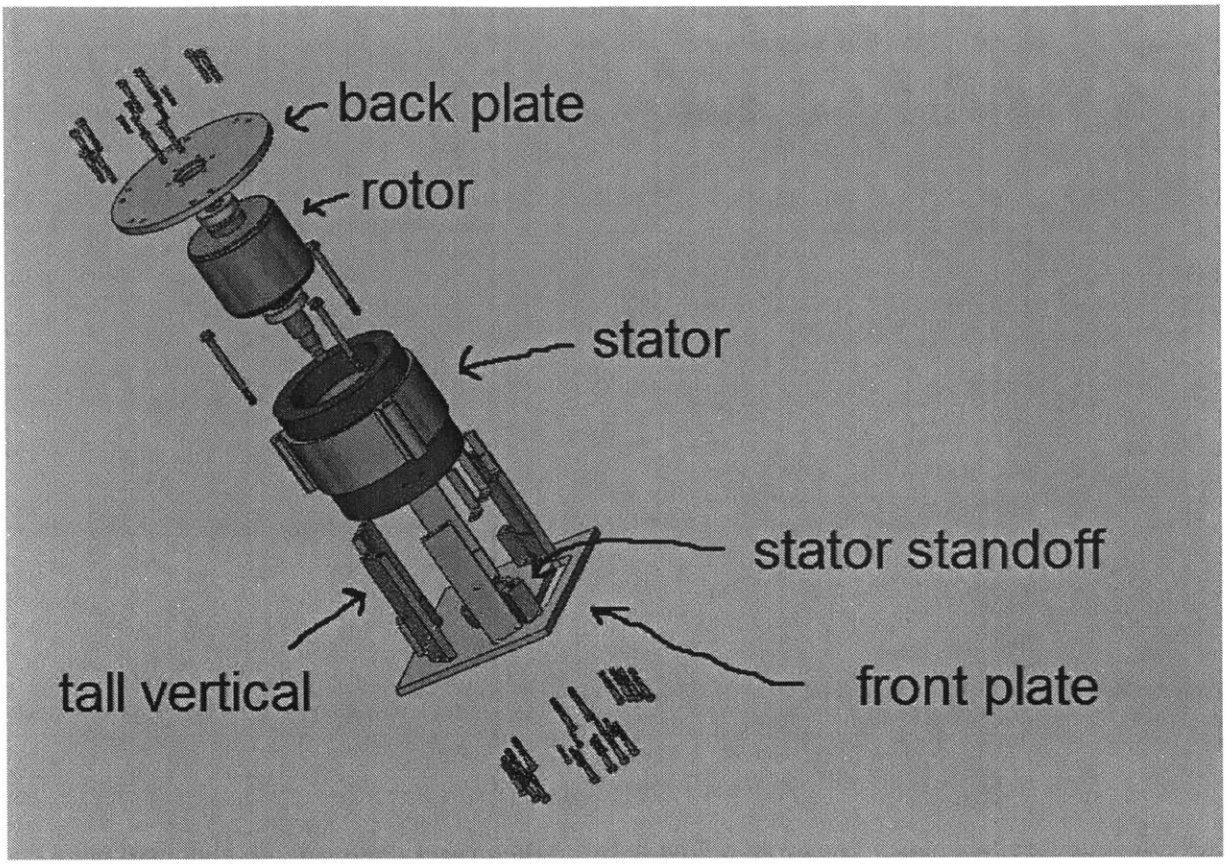

Figure 9: Model of motor housing.

Motor housing manufacture

Working from the computer models, the metal parts were machined. The material used is mostly 6061 aluminum, with some unidentified scrap aluminum used for the tall verticals and the bearing housings. Knowing that some aluminum alloys do not weld well, the strength of welds to the unidentified scrap was confirmed before committing to use it in the assembly.

The cap screws attaching the tall verticals and stator standoffs to the front plate are used primarily for fixturing during welding.

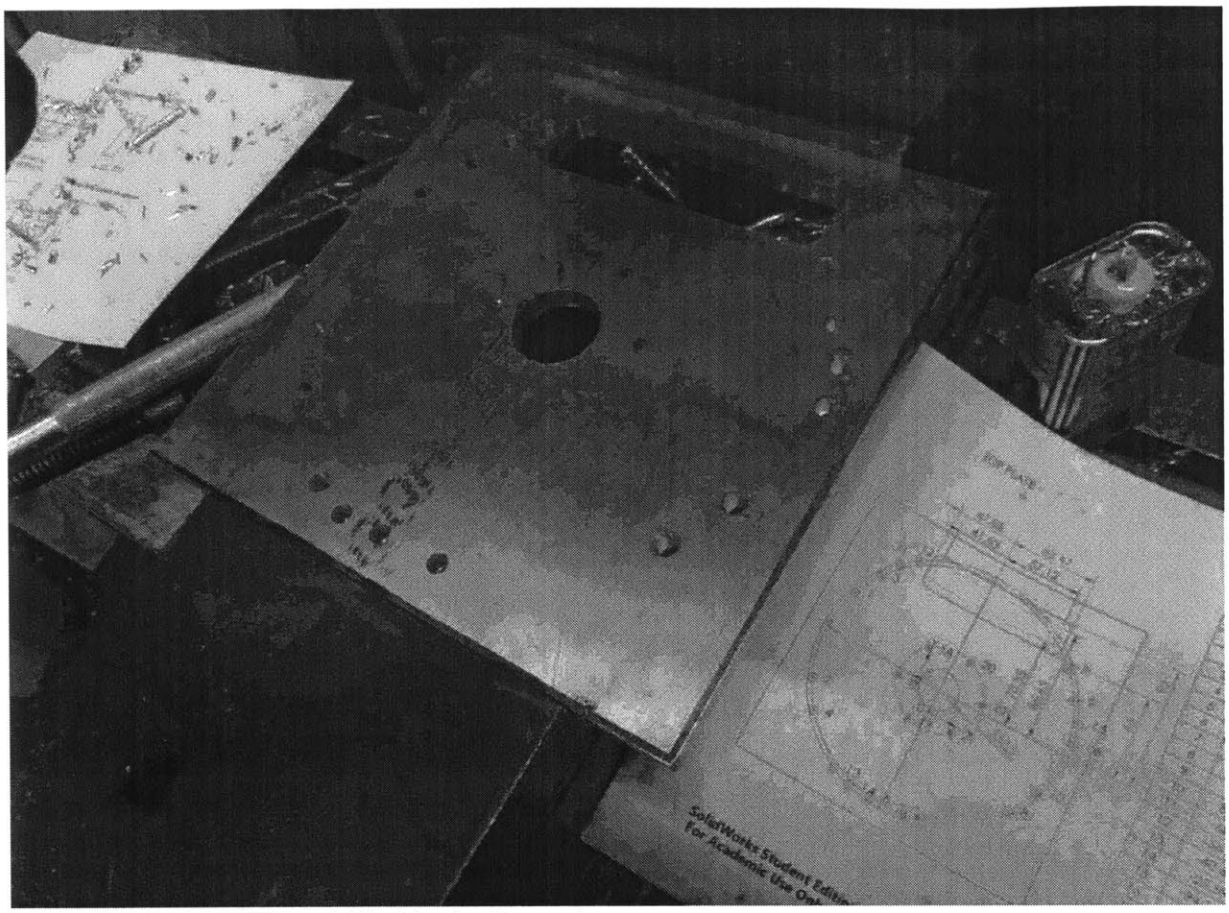

Figure 10: holes being drilled in the front plate
The vertical members were machined to length, drilled and tapped, and attached to the front plate with socket head cap screws.

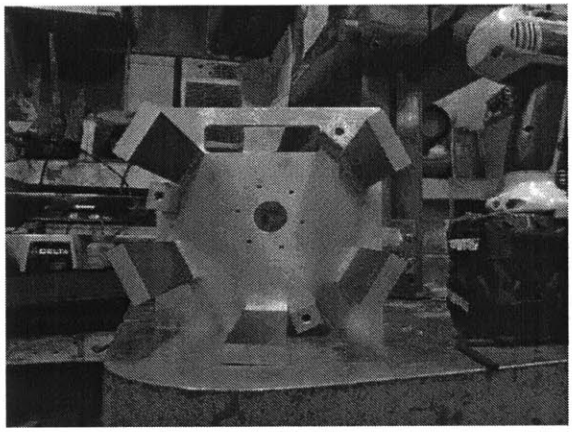

Figure 11: unbored motor housing, top view

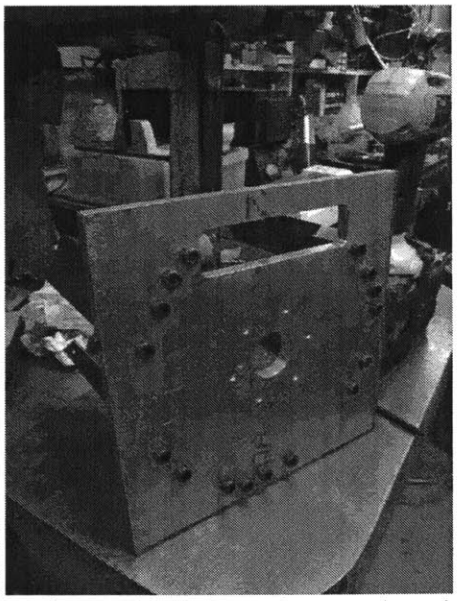

Figure 12: unbored motor housing, bottom view

Next, unbored bearing housings were welded to both the front and back plates, and all of the vertical members were welded to the front plate. Welding was done on a Miller Dimension 200 TIG with 80% electrode negative AC balance. The 3/8" thick plate and stout stator standoffs were at the limit of this welder's capability, so the metal did not flow until the entire workpiece was hot to the touch.

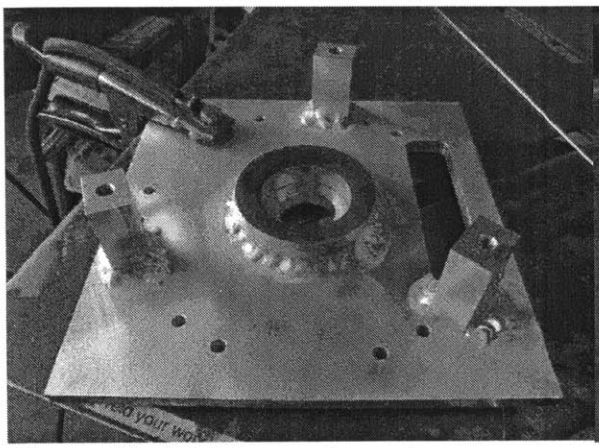

Figure 13: Welding to front plate

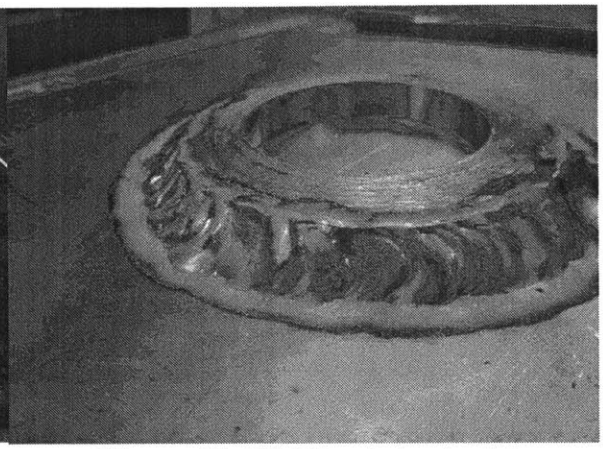

Figure 14: Welding to back plate

Next, the minor diameter of the stator was milled into the tall verticals using a rotary table and a long 1" diameter end mill. The nod and tilt of the mill head were zeroed prior to this step. The three stator mounting holes were used for locating and centering the part on the rotary table.

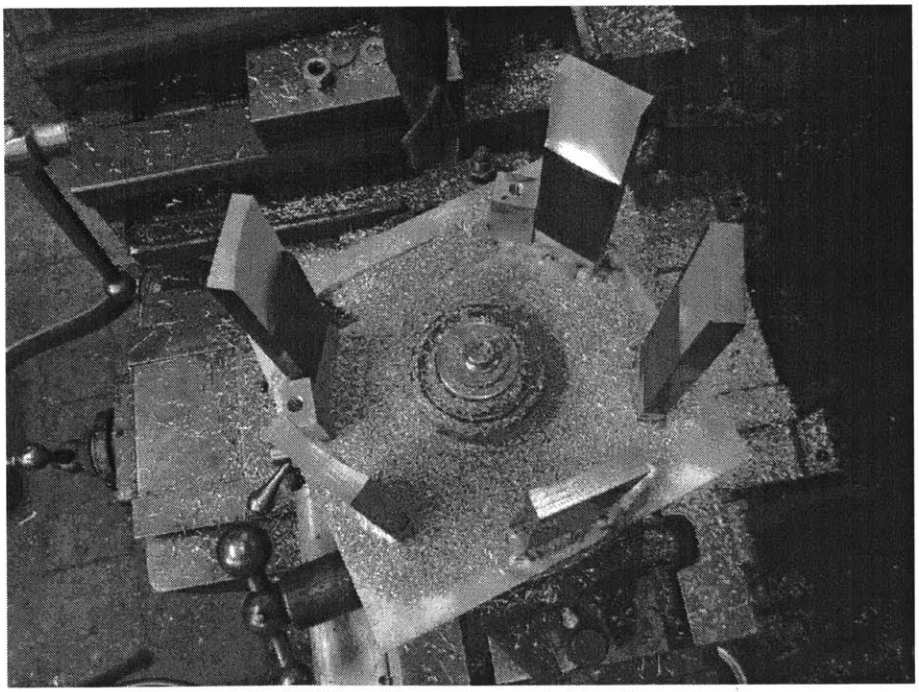

Figure 15: Milling the stator outside diameter bore

The fit of the stator was confirmed before removing the front plate assembly from the rotary table. Once removed, the verticals were filed to clear the stator lobes and allow the through holes in the stator laminations to align with the tapped holes in the front plate assembly. The stator was then attached with M8 hex head cap screws and washers. The entire assembly including the stator was then clamped in the mill vise and a piece of brass wire was used as a feeler to find the center of the stator. The brass wire was held in a drill chuck. It was manipulated along with the X and Y axes of the milling machine until it barely scraped the stator bore around the entire circumference. Using the DRO on the milling machine, it was confirmed that this operation found center to within 0.03 mm. For reference, the nominal rotor-stator airgap on this machine is approximately 0.5 mm.

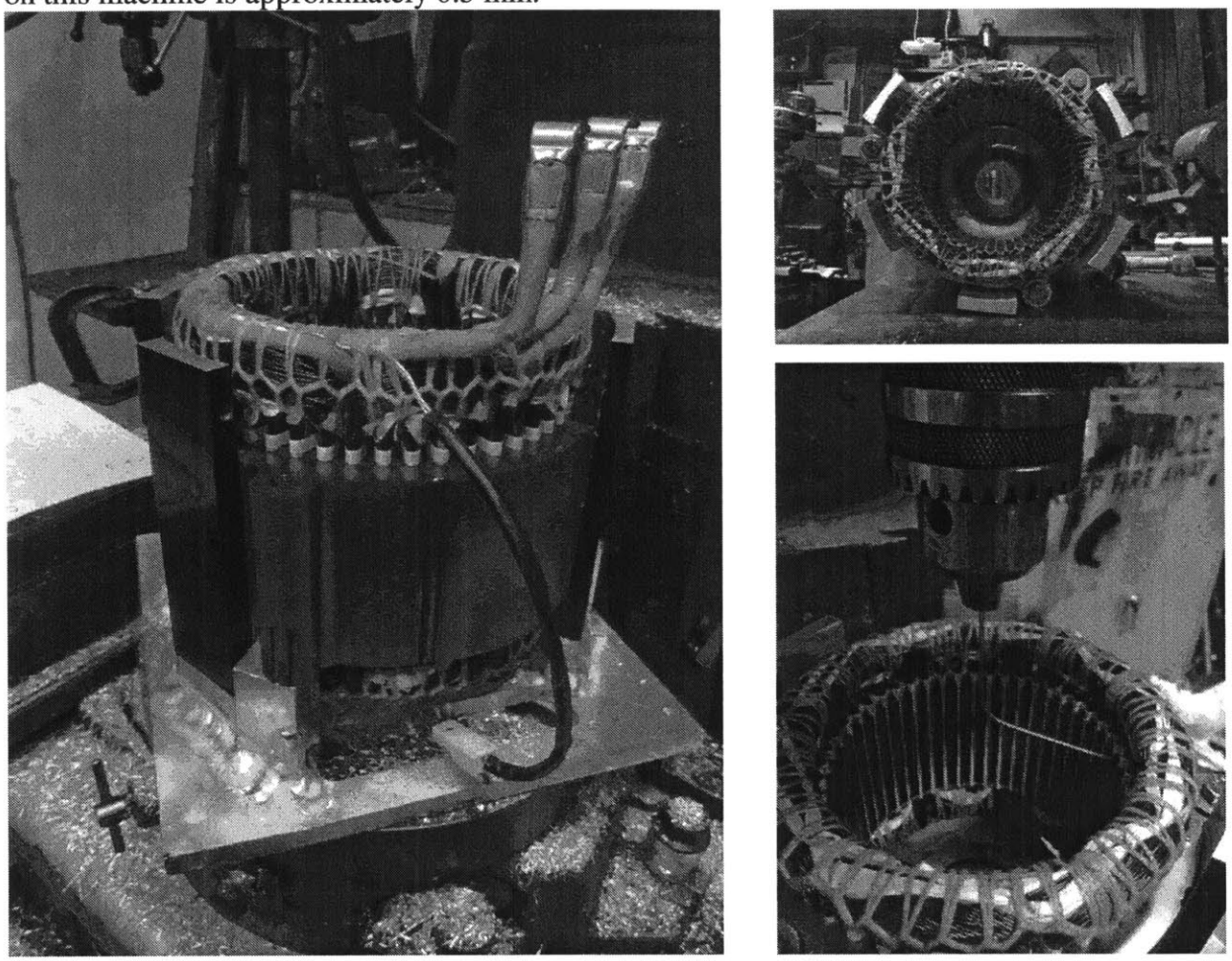

Figure 16: Preparing to machine lower bearing bore

With the center located, spring pins and tapped holes were made for locating and fixturing the back plate. Next, the stator was removed and the front bearing bore was machined using a boring head.

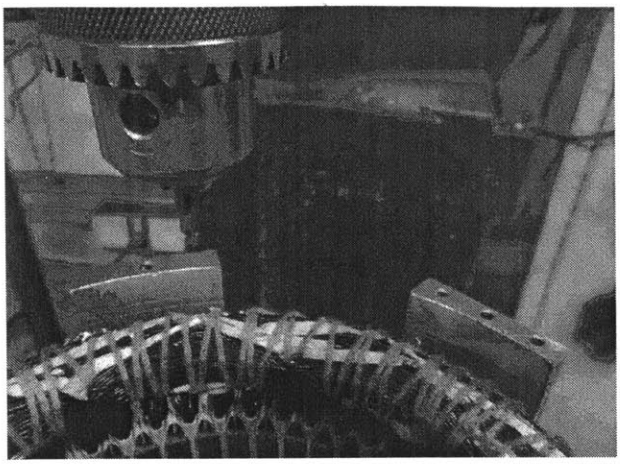

Figure 17: drilling holes for back plate mounting

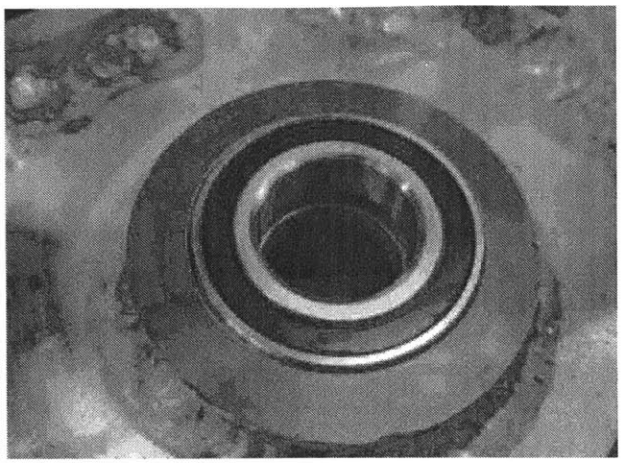

Figure 18: completed front bearing bore

Because this machine was designed to be run in a bath of filtered oil, the original rotor bearings were unsealed. Additionally, the machine's bearings were not specified to take significant radial loading as output power was originally carried through a spline to a geared jackshaft with its own bearings capable of taking radial loads. As further testing was to take place in open air with potentially significant radial loads from a belt or chain, the unsealed rotor bearings were replaced with larger sealed bearings sold inexpensively as ATV wheel bearings. The speed and load ratings of the new bearings were confirmed to be adequate.

The original bearings were pressed on tightly with little clearance to insert a bearing puller. They were cut off with a small abrasive wheel. The rotor was covered in painters tape to ease the removal of the magnetic iron particles created during cutting. Inadvertently, this revealed the location of the magnets within the rotor. It is interesting to note the small angular offset that occurs midway through the lamination stack. Similar things are done in the rotors and stators of other electric machines to reduce cogging torque and torque ripple.

Figure 19: Removing the unsealed bearings

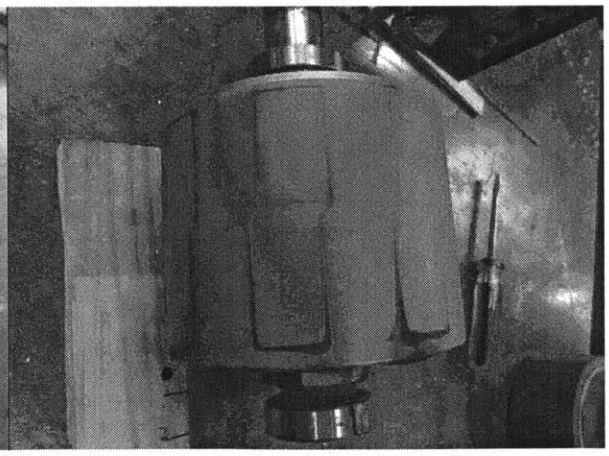

Figure 20: magnetic dust on the rotor

Next, the back plate bearing bore was machined and the spring pin holes and through holes were drilled. The new bearings were pressed on to the rotor shaft and the machine was assembled.

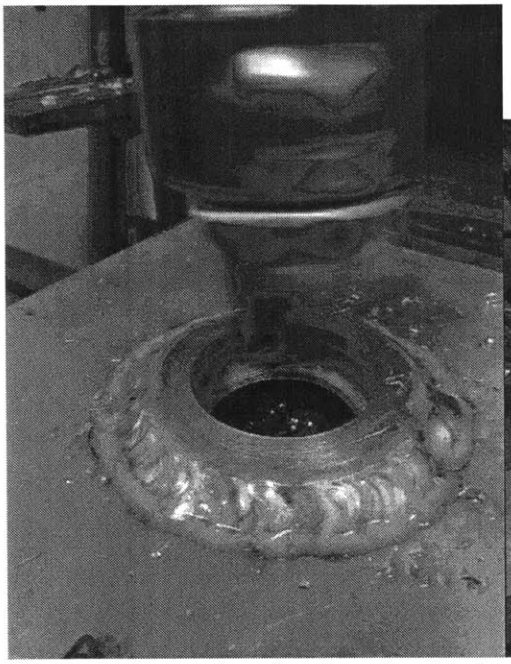

Figure 21: rear bearing housing boring

Figure 22: testing the rotor fit

Initial Testing

To test that the rotor spun quietly and freely, the first test was performed with a small sensorless motor controller. This 500W Chinese electric bicycle controller is available on ebay for $40 or less. It very reliably spins most three phase permanent magnet machines without needing external rotor position detection sensors.

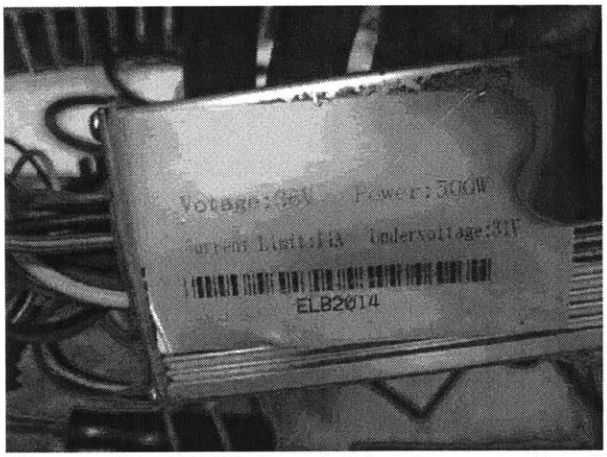

Figure 23: 500W electric bicycle controller

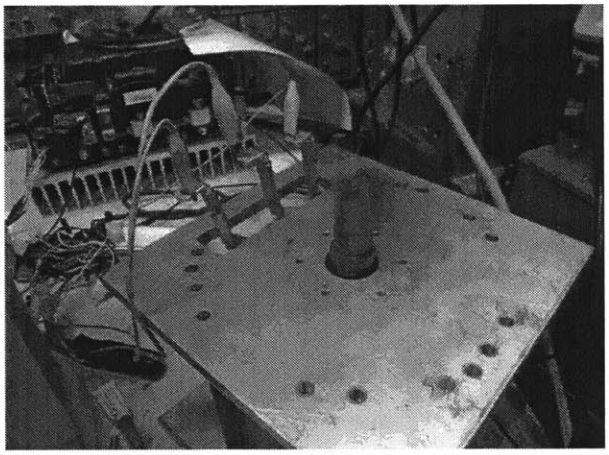

Figure 24: MG1 being driven by bicycle controller

Measured Characteristics

A line-to-line back-EMF signal was measured by spinning the motor up to speed with the sensorless controller, then disconnecting the controller and quickly capturing a trace while the machine decelerated.

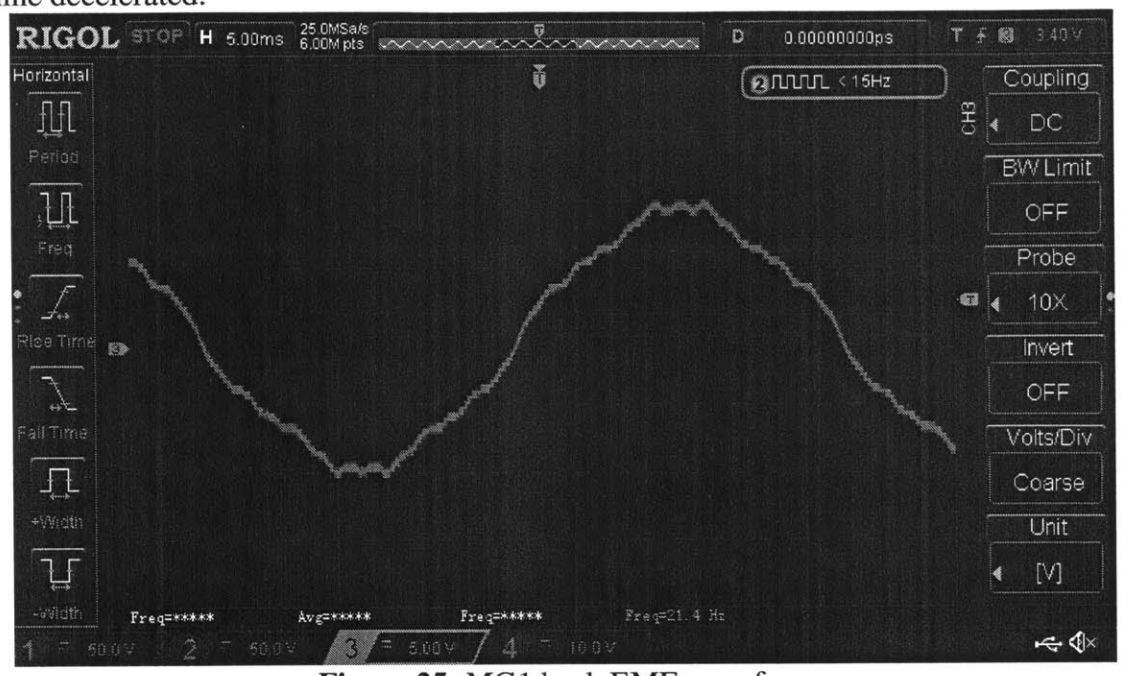

Figure 25: MG1 back EMF waveform

Because the rotor of this machine has four pole pairs, its electrical frequency must be four times its mechanical frequency. To calculate Kv from the information in the scope trace above, the following equation was used. N is the number of rotor pole pairs, $f_{electrical}$ is the fundamental frequency of the back EMF signal, and V_{pp} is its peak to peak voltage.

$$Kv\left[\frac{rad/s}{V}\right] = \frac{\omega_{mechanical}\left[\frac{rad}{s}\right]}{V_{pp}} = \frac{\omega_{electrical}\left[\frac{rad}{s}\right]}{N} * \frac{1}{V_{pp}} = \frac{2\pi * f_{electrical}[Hz]}{N * V_{pp}}$$

Phase to phase winding resistance was measured using the four wire method. 1 amp of current was run from one phase terminal to another and the voltage drop was measured with a voltmeter. This measurement of phase resistance depends on the unconfirmed assumption that these motors are wye terminated. Large motors designed for high efficiency are typically not delta wound due to the additional resistive losses incurred by circulating currents. [3, pp. 63-4]

Physical and electrical characteristics are recorded in the tables below. For comparison, specifications of the motor/generators in a 2004 Toyota Prius are also listed.

Electrical Characteristics	Kv [3] $\left(\frac{rad}{V*s}\right)$	Kt $\left(\frac{N*m}{A}\right)$	Winding resistance, phase to phase $(m\Omega)$	Km $\left(\frac{N*m}{A*\sqrt{\Omega}}\right)$
2011 Mercury Milan MG1	1.6	0.63	23.4	4.1
2004 Toyota Prius Generator [4]	2.1 [5]	0.48	96.8 [6]	1.5
2004 Toyota Prius Motor	0.077	13	138	35

The motor back EMF constant Kv, with units of $\frac{V*s}{rad}$ can be inverted to yield the torque constant, Kt with units of $\frac{N*m}{A}$. However, in an interior permanent magnet (IPM) machine, the Kt found in that way will not represent the reluctance torque that comes with the addition of stator current to the direct axis. It will only represent the torque that results from the interaction of the rotor permanent magnets with magnetic fields resulting from quadrature axis stator current (as is the case in a surface permanent magnet motor). Figure <> shows that torque in an IPM machine is a combination of magnet torque and reluctance torque.

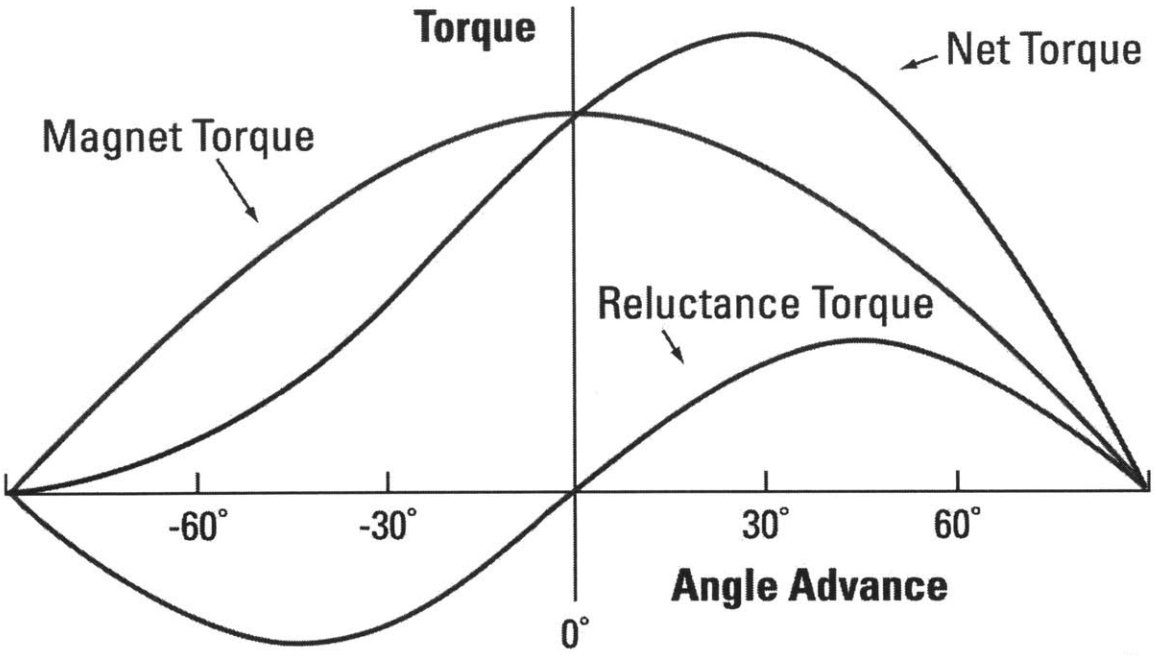

Figure 26: summation of magnet and reluctance torques in an IPM machine [7]

[3] Kv, the ratio between back EMF and rotor speed, is commonly expressed using units of RPM/V or (rad/s)/V. Many people find RPM to be a more intuitive expression for rotational speed than rad/s. However, (rad/s)/V are convenient units because the quantity can be inverted to yield Kt, the torque constant, in units of N*m/A. To convert from RPM/V to (rad/s)/V, multiply by $\frac{2\pi\left(\frac{radians}{revolution}\right)}{60\left(\frac{seconds}{minute}\right)}$. Conveniently, $\frac{2\pi}{60} \approx 0.1$

[4] Unless noted otherwise, all Prius data is from this 2010 ORNL report: http://info.ornl.gov/sites/publications/files/Pub26762.pdf

[5] This point from this 2004 ORNL report: http://www.engr.uvic.ca/~mech459/Pub_References/890029.pdf

[6] http://www.searchautoparts.com/motorage/electrical/toyota-prius-transaxle-group-case-study

[7] EE Times. *Design platforms enable variable-speed motor control in energy-efficient appliances.* http://www.eetimes.com/document.asp?doc_id=1272381

Physical Characteristics	Rotor Mass (Kg)	Stator Mass (Kg)	Rotor Pole Pairs	Stator Teeth
2011 Mercury Milan MG1	6.5	13.2	4	48
2004 Toyota Prius Generator	4.01	9.16	4	48
2004 Toyota Prius Motor[8]	10.2	25.9	4	48

Inside the Prius Inverter Assembly

At the time of writing, second and third generation Prius inverter assemblies can be purchased for about $150 on Ebay and through used parts dealers. The second generation Prius inverter assembly is shown below with the cover removed. The locations of connectors are labeled.

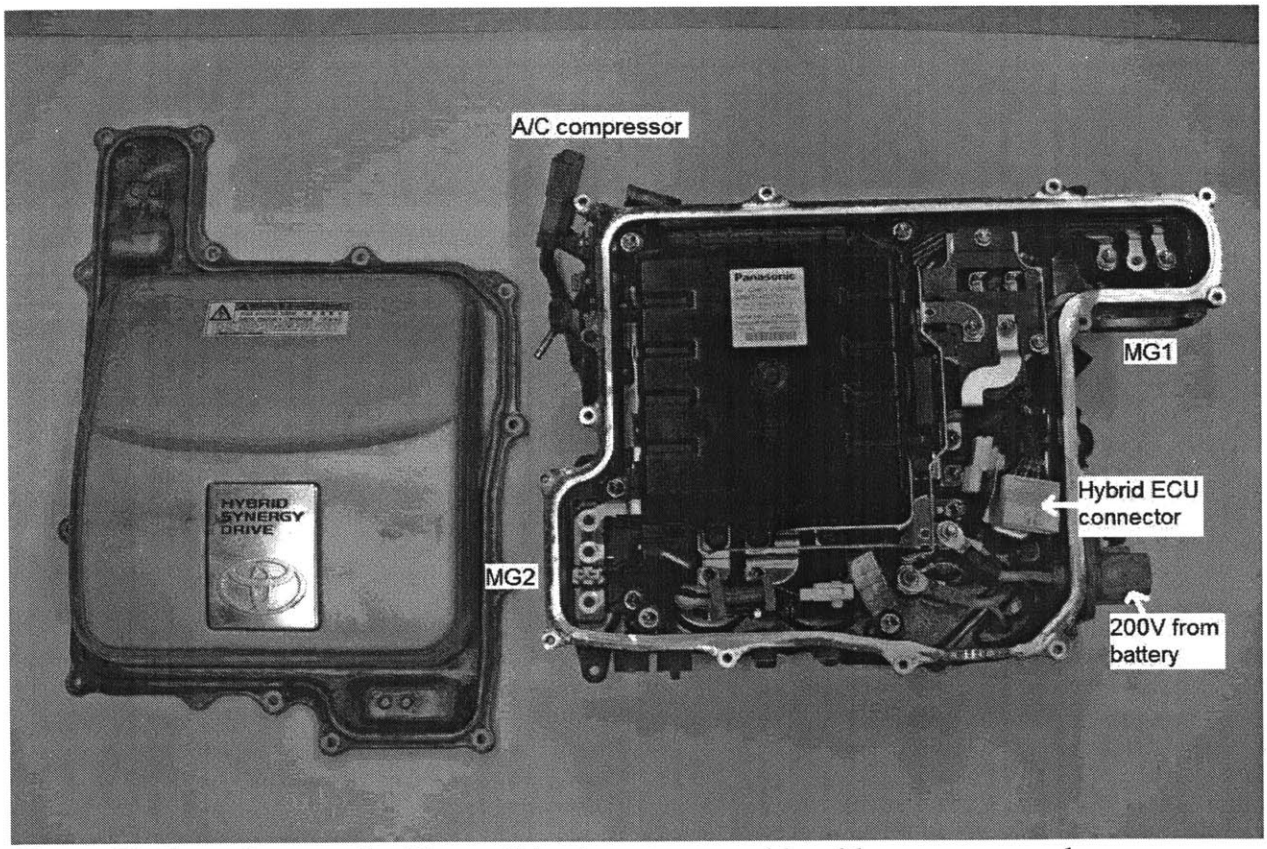

Figure 27: Second generation Toyota Prius inverter assembly with cover removed

[8] See [3]

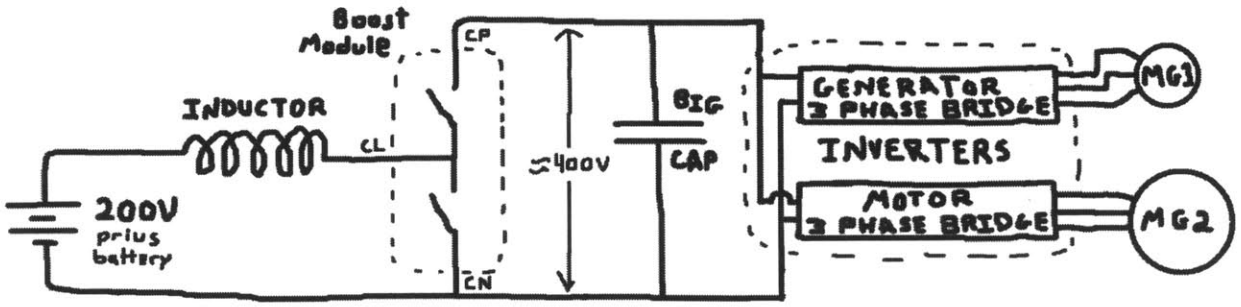

Figure 28: Schematic of power electronics in the second generation Toyota Prius inverter assembly

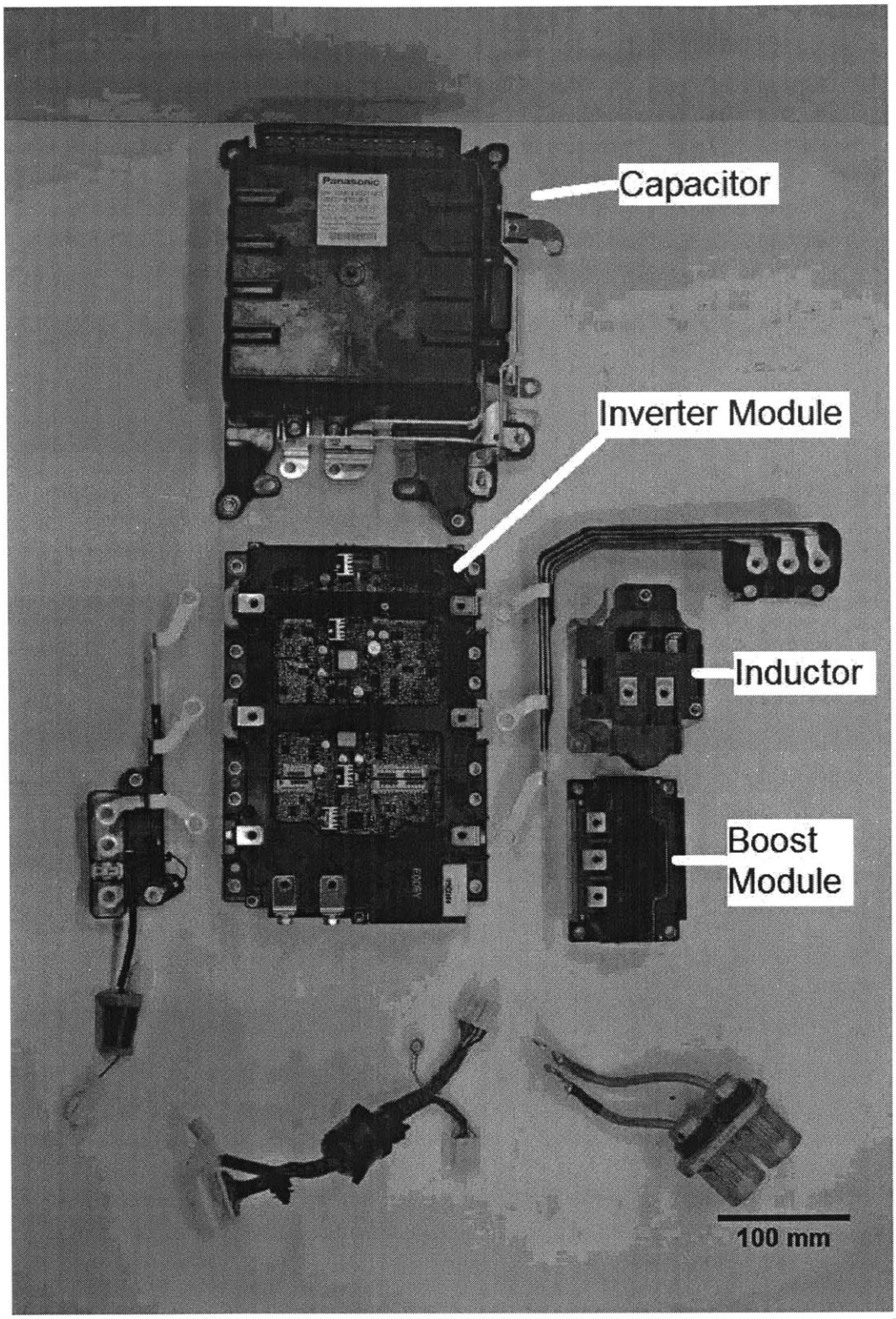

Figure 29: Major components in the second generation Toyota Prius inverter assembly

Significant analysis of the inverter assembly has already been performed and documented. Most notable is a 2006 report by ORNL called *Evaluation of 2004 Toyota Prius*

Hybrid Electric Drive System[9] However, even in the hobbyist sphere, there has been little information published on how to actually use the object for its intended purpose.

Use of the second generation Toyota Prius inverter

The inverter module contains a pair of three phase bridges, one for the generator and one for the motor. The power stage is electrically isolated from the control inputs. Conveniently, a pinout for the inverter module is printed on the circuit board. The service manual[10] contains descriptions of what the voltage on each pin should look like during normal operation. Based on our testing, the module runs happily between 10 and 20 volts. It likely contains a switched mode power supply as current draw drops as supply voltage is increased. It draws about 12 watts at idle. Each gate driver almost certainly has its own isolated power supply. It contains two current sensors on each three phase bridge. That is adequate for three phase motor control as it is assumed that the currents sum to zero. The third current can be calculated from the first two. The current sensors on the motor side are rated to +/- 400A and those on the generator side are rated to +/- 200A. We found during testing that the inverter shuts down and floats the phases when phase current on either side exceeds the rating of its current sensor.

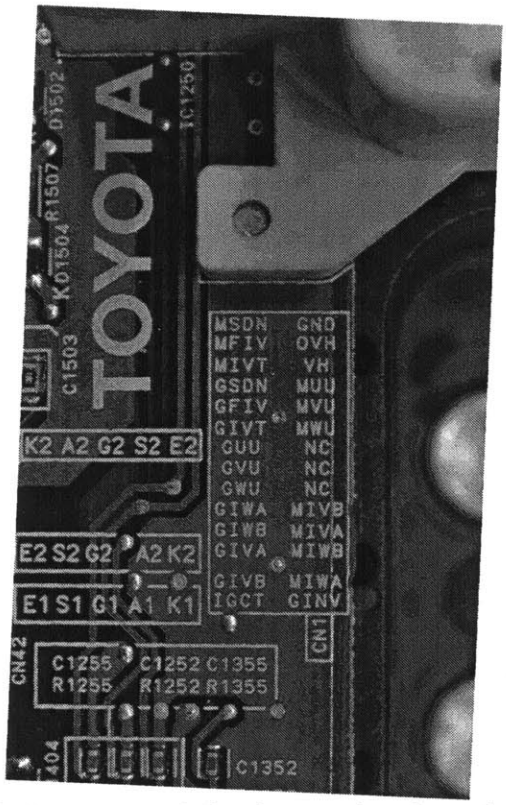

Figure 30: Inverter module pinout printed on circuit board

[9] http://www.engr.uvic.ca/~mech459/Pub_References/890029.pdf
[10] Relevant screenshot posted here: http://techno-fandom.org/~hobbit/cars/ginv/terecu/list.html

Initial powered tests of MG1 were done with a Chinese electric bicycle controller capable of sensorless control. The next task was to spin MG1 with the Prius inverter. A friend and colleague had already put significant work into this part of the project, purchasing a used Prius inverter and figuring out how to turn it on, as well as making an Arduino-based inverter controller capable of performing six-step block commutation on a small motor equipped with latching hall effect sensors.

For control of the larger motor, we decided to implement a form of current control called field oriented control (FOC). An explanation of FOC is beyond the scope of this paper (an excellent one can be found in [3]). It was chosen because it provides smoother low speed operation and better regulation of current than block commutation.

Rotor Position Detection

Lacking the stator and drive electronics for the VRR rotor present on the shaft left the options of either reproducing those components or seeking an alternate method of position detection. A prototype VRR stator was produced, but that approach was dropped after failing to find an inexpensive Resolver to Digital (R2D) IC.

Three latching hall sensors are often used for rotor position detection on small permanent magnet motors such as those found in CD drives, electric bicycles, and scientific and industrial applications where position information is needed for control. Each of the three latching hall sensors has two states for a total of $2^3 = 8$ states. Two of those states (1,1,1 and 0,0,0) are invalid, and each of the other six corresponds to a 60 degree sector of a circle. Knowing rotor position to within 60 degrees is enough to reliably command a torque in a known direction.

Latching hall sensors (figure <>) were installed between the stator teeth of MG1 (figure <>) to detect the fringe fields of the rotor. They were placed 120 electrical degrees apart. Because the rotor has four pole pairs, 120 electrical degrees corresponds to 120/4 = 30 mechanical degrees.

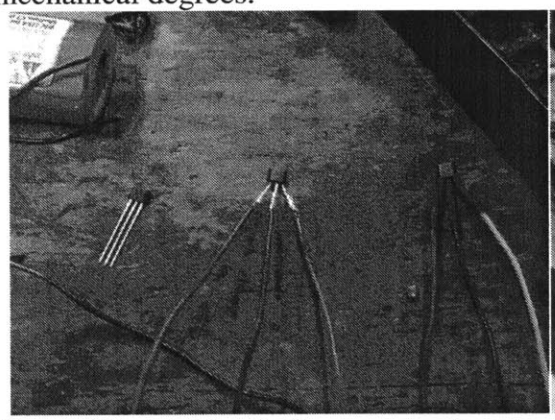

Figure 31: latching hall sensors and wiring

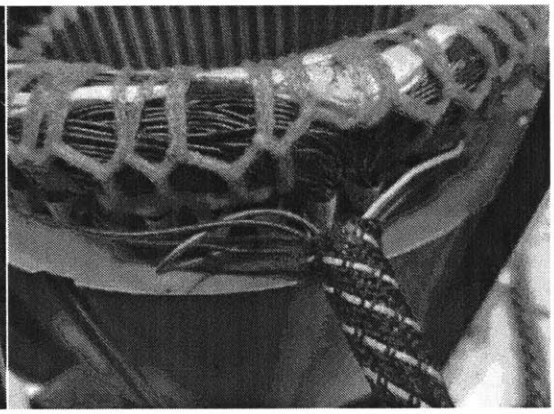

Figure 32: hall sensors installed in MG1 stator

Detecting the rotor fringe fields proved to be unreliable. Figure <> shows the three hall sensor outputs. They were unusable, likely due to inconsistent rotor fringe fields.

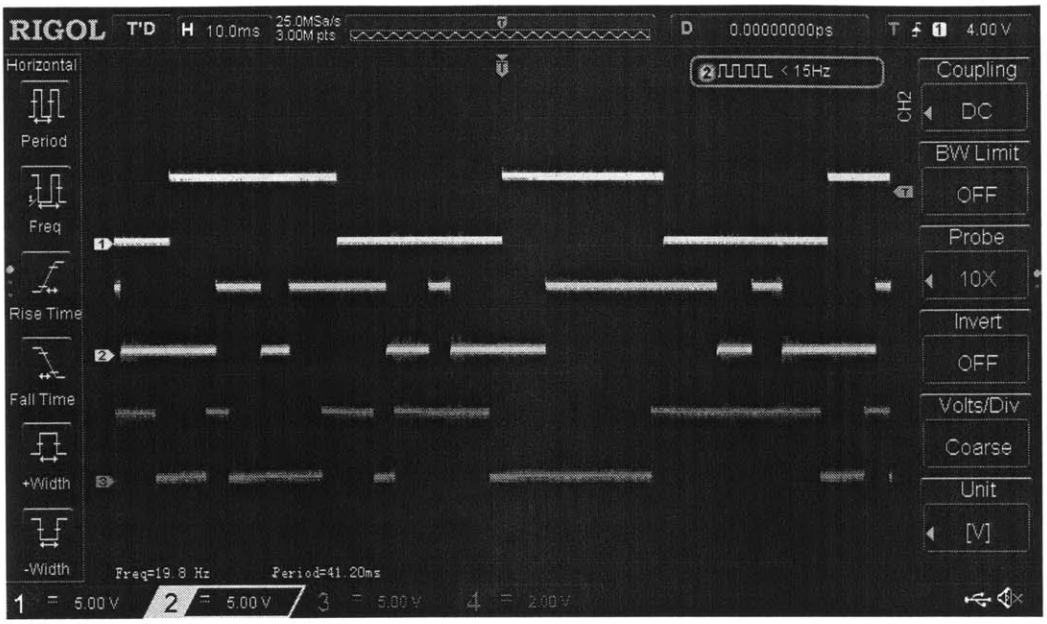

Figure 33: unusable latching hall sensor outputs

This problem was worked around by attaching an auxiliary magnet array to the rotor for the sole purpose of position detection. The array is made of magnets pressed into a printed ABS carrier. A turned acetal plug (black) is pressed into the hollow end of the MG1 rotor shaft.

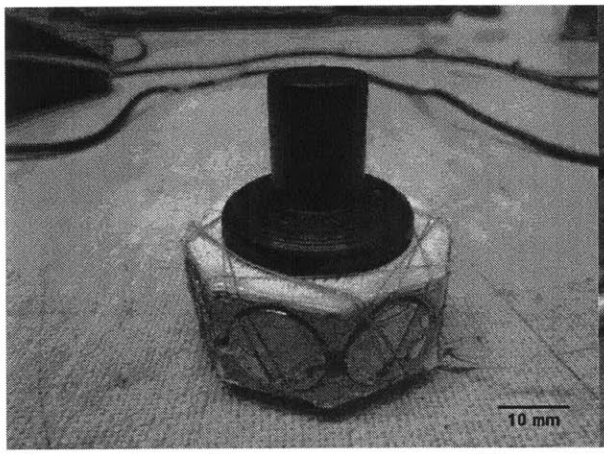

Figure 34: auxiliary magnet array

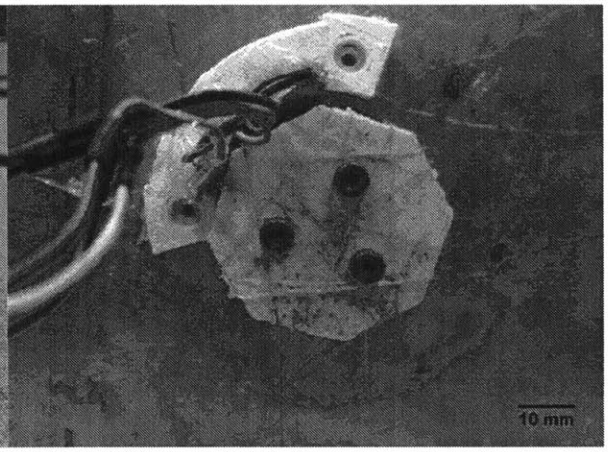

Figure 35: installed magnet array and latching hall sensors

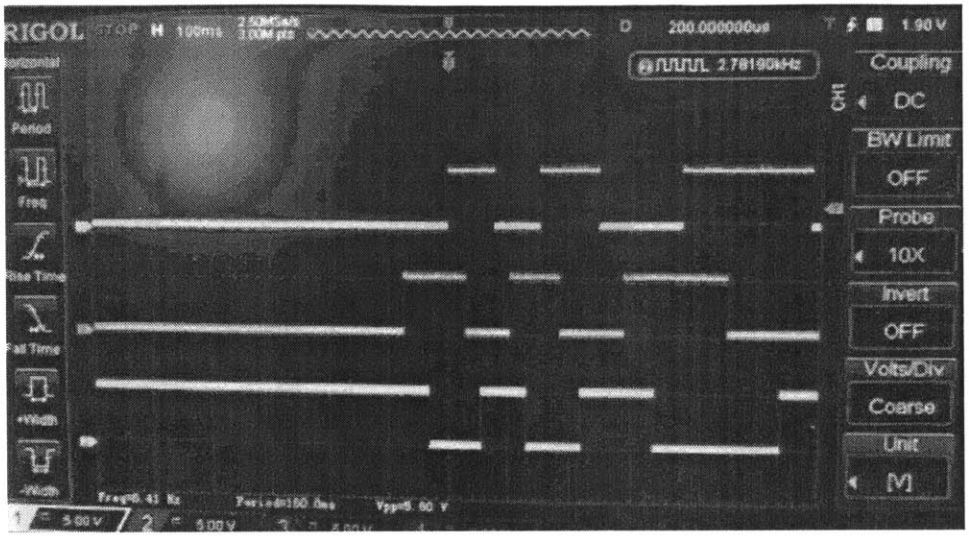

Figure 36: Output of hall sensors detecting the auxiliary magnet array at varying rotor speed

The external array produced satisfactory output. As development of the control scheme progressed towards FOC, it became apparent that having finer rotor position detection would simplify the controller. As the industry standard VRR solution would have been difficult to replicate, a workaround capable of producing similar output waveforms was produced. Using the existing external magnet array, a new absolute position detection system was implemented using two Allegro A1324 analog hall sensors.

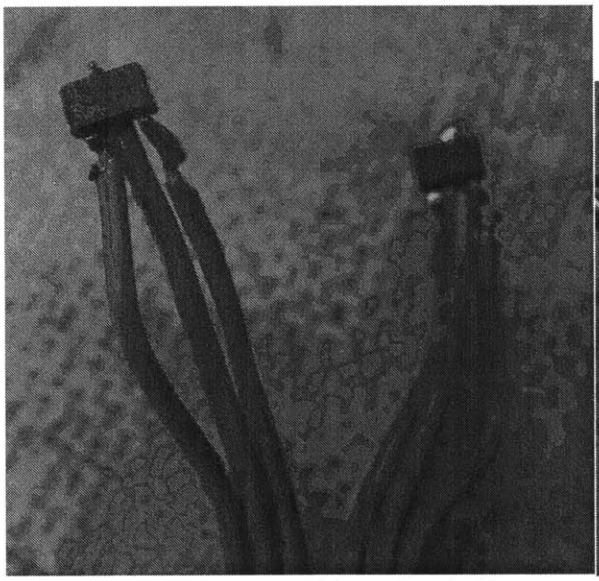

Figure 37: Allegro A1324 analog hall sensors

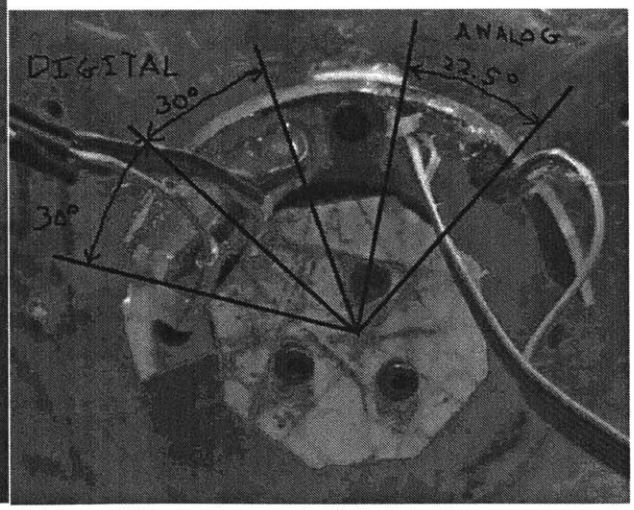

Figure 38: analog and digital hall sensor spacing

The analog hall sensors were positioned with respect to the external magnet array such that they would pass sinusoids of similar magnitude with approximately 90 degrees of phase offset. These outputs are similar to the sine and cosine outputs of the resolvers used in hybrid cars and elsewhere.

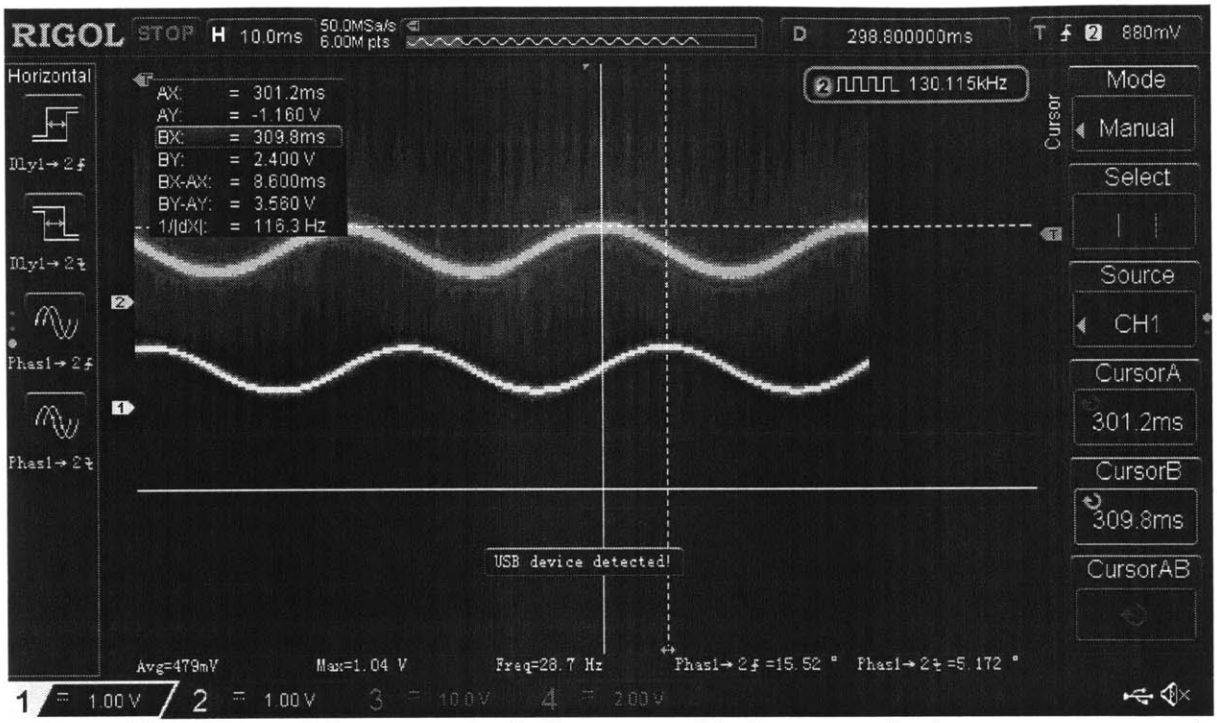

Figure 39: Outputs of the two analog hall sensors with the rotor spinning at constant speed

Using the two components, absolute angle is calculated by taking their arctangent.

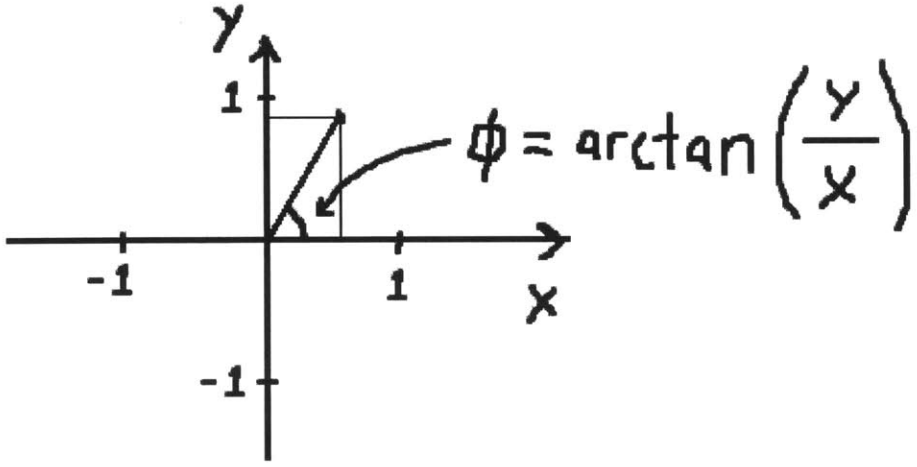

Figure 40: calculation of arctangent using sine and cosine components

This calculation was performed on a microcontroller. A sample of the code is shown below.

```
57
58          motor->analoga = analoga;
59          motor->analogb = analogb;
60
61
62          float ascaled = 2*(((motor->analoga-0.143)/(0.618-0.143))-0.5);
63          float bscaled = 2*(((motor->analogb-0.202)/(0.542-0.202))-0.5);
64
65          float x = bscaled/ascaled;
66
67
68          unsigned int index = ((abs(x))/(M))*ATAN_TABLE_SIZE;
69
70          if(index>2000)index=2000;
71
72
73          if(bscaled<0){
74              if(ascaled<0) motor->whangle = arctan[index];
75              if(ascaled>0) motor->whangle = 180 - arctan[index];
76              }
77
78          if(bscaled>0){
79              if(ascaled>0) motor->whangle = 180+ arctan[index];
80              if(ascaled<0) motor->whangle = 360- arctan[index];
81              }
82
83          if(motor->whangle>360)motor->whangle=360;
84          if(motor->whangle<0)motor->whangle=0;
85
```

Figure 41: code to convert raw analog hall values to rotor angle

Lines 62 and 63 scale the raw analog hall sensor inputs so that they range from -1 to 1. The calibration values were found manually by recording a serial stream of raw values and finding the minima and maxima. Line 65 divides one value by the other. The quotient is then used to look up the corresponding arctangent value in a table. Since arctangent returns a value between 0 and 90 degrees, the conditional statements in lines 73-81 are necessary to find which quadrant the point lies in.

A plot of position data logged over serial is shown below. The motor is being driven open loop.

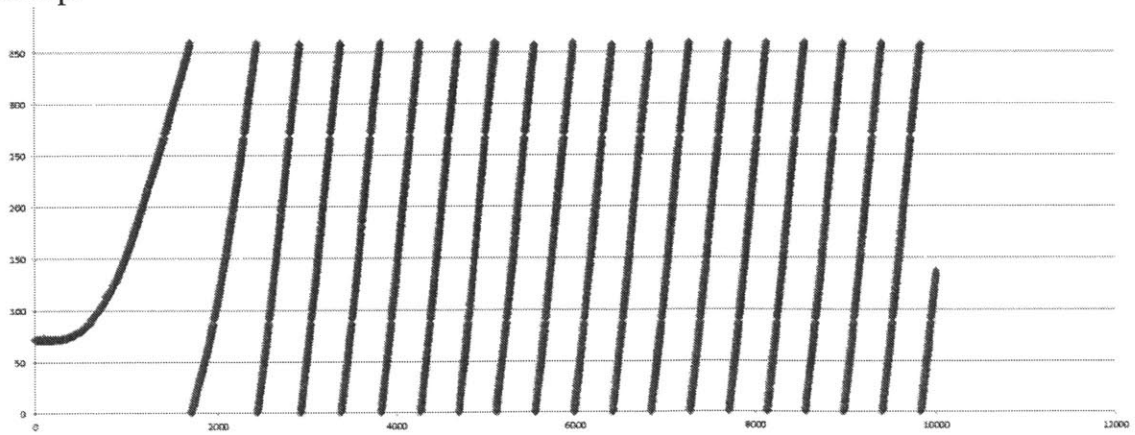

Figure 43: Usable angle ramp from analog hall position detection method logged over serial

With this method of position detection proven to be functional, a more compact and robust magnet array and sensor housing was made.

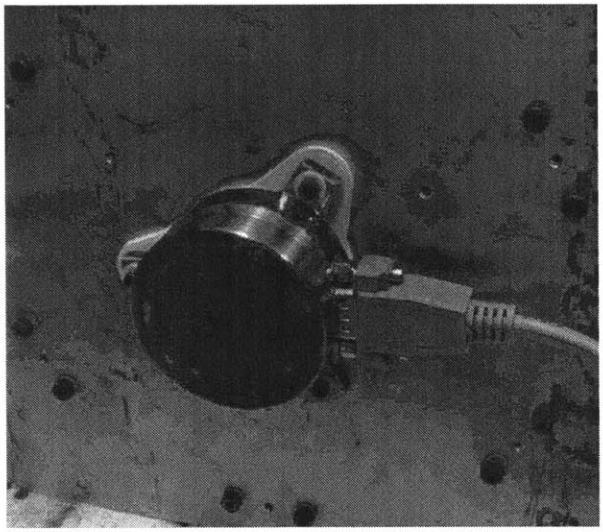

Figure 44: steel sensor housing

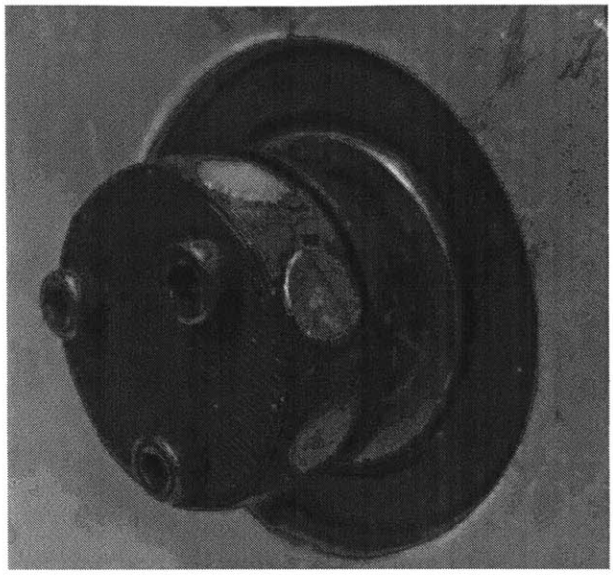

Figure 45: compact auxiliary magnet array

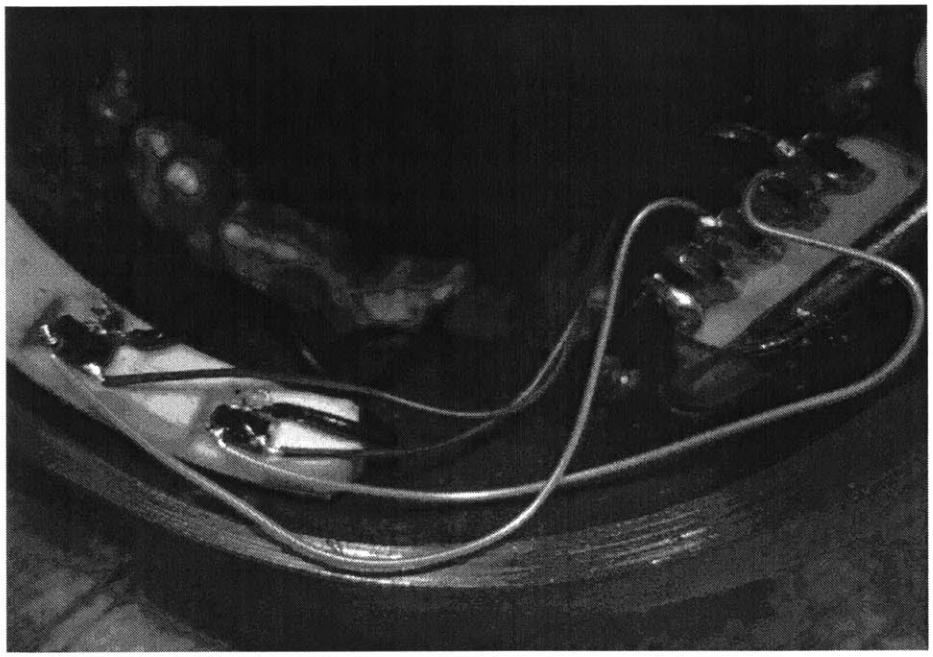

Figure 46: Detail of analog hall position sensor wiring

Significant noise was coupled into the system when the motor housing was put into electrical contact with the logic ground. This was mitigated by electrically isolating the sensor housing from the motor housing with printed spacers.

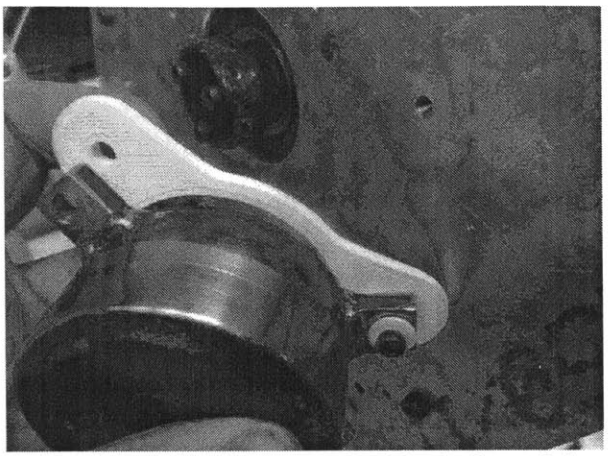

Figure 47: printed ABS spacers for electrical isolation of the sensor housing

Controller Hardware

The controller is based on the STM Nucleo F411RE development board. The board has the footprint of an Arduino Uno, uses a cloud compiler, and costs ten dollars. Attached to that is a board developed by my collaborator. It contains output buffers, input voltage dividers and analog filters for interfacing with the inverter, the rotor position sensors, and the user's throttle input.

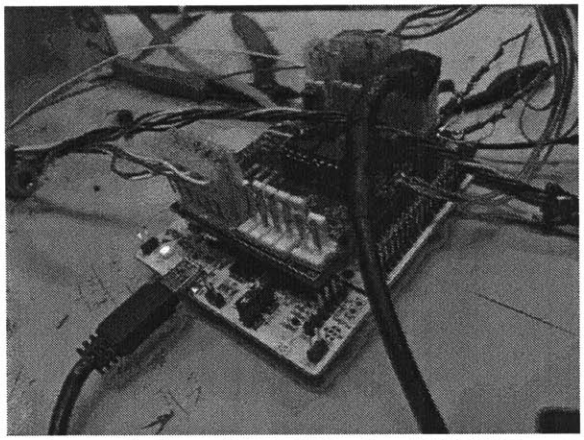

Figure 48: Hardware stack consisting of STM Nucleo F411RE and a custom I/O board for communicating with the motor and inverter

Implementation of Field Oriented Control

Unfamiliar with FOC, my colleague and I studied application notes to find details on how to implement it. *AN1078* from Microchip[11] proved adequate. The relevant block diagram is reprinted below

[11] http://ww1.microchip.com/downloads/en/AppNotes/01078B.pdf

FIGURE 6: VECTOR CONTROL BLOCK DIAGRAM

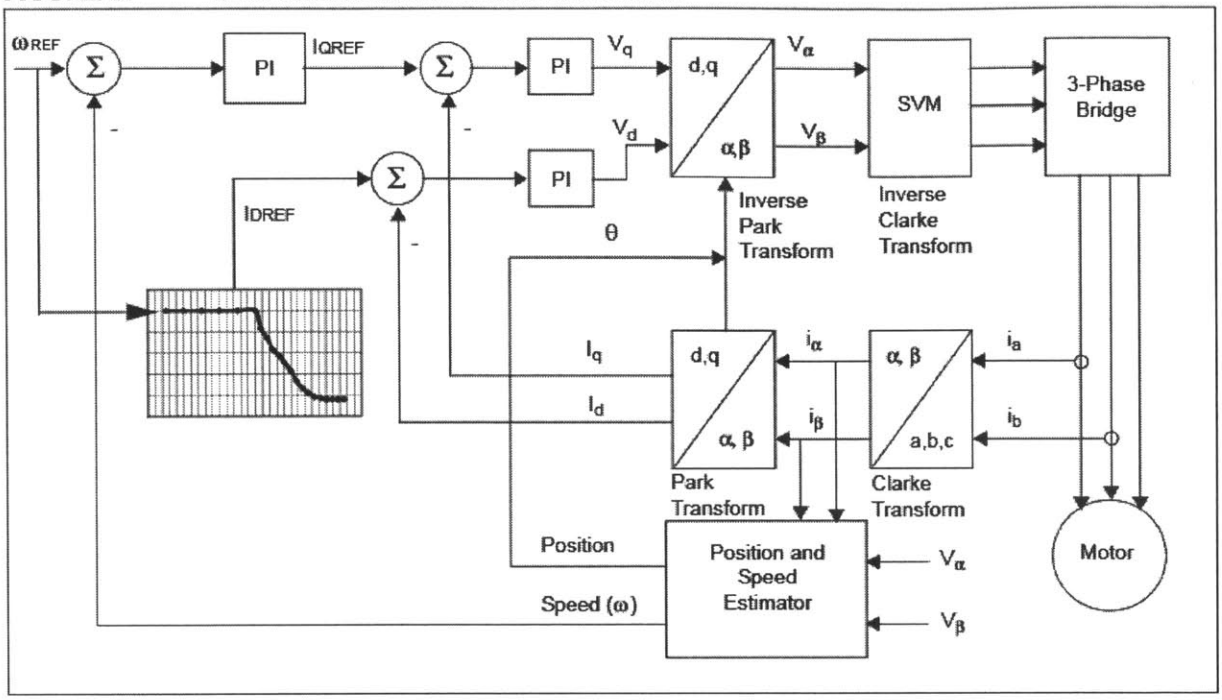

Figure 49: block diagram of FOC from [11]

The Microchip application note covers sensorless FOC, meaning that it doesn't assume the use of a dedicated position sensor. Using a position sensor like the one developed earlier significantly simplifies the implementation of FOC because it eliminates the need for estimation of rotor position and speed using only phase voltages and currents.

Implementing FOC was a sometimes-quite-difficult multi-week process. A block would be written and tested by logging data over serial. Getting it to work would often involve changing signs, checking math, and finding errors in previous blocks. Sequential debugging of the duty cycle outputs produced by the space vector modulator block is shown in the series of graphs below

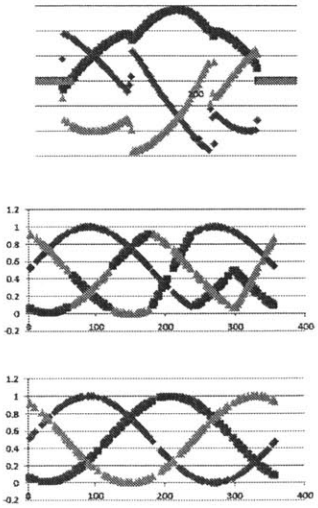

Figure 50: debugging of the space vector modulator until it produces smooth sinusoids

Construction of a flywheel assembly began soon after the loop began showing signs of working correctly. The purpose of the flywheel assembly was to see how the system would perform given a small load.

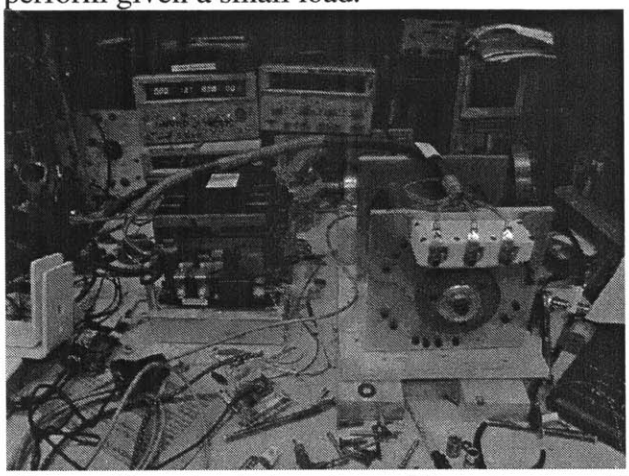

Figure 51: unloaded motor and inverter

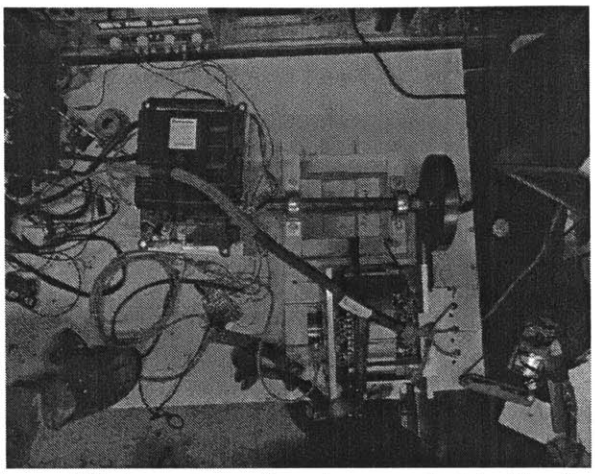

Figure 52: top view of motor coupled to flywheel

Again, more data was logged via serial and more errors were corrected.

Construction of demonstration vehicle

My colleague and I had been searching for donor vehicles since the start of the project, months ago. We concluded that the size and power range of the system best fit a small motorcycle or dirtbike. The project fell dormant for a week with a functional system and nowhere to put it. We were extremely fortunate to be given an engineless 1986 Yamaha XT-350 frame by a friend.

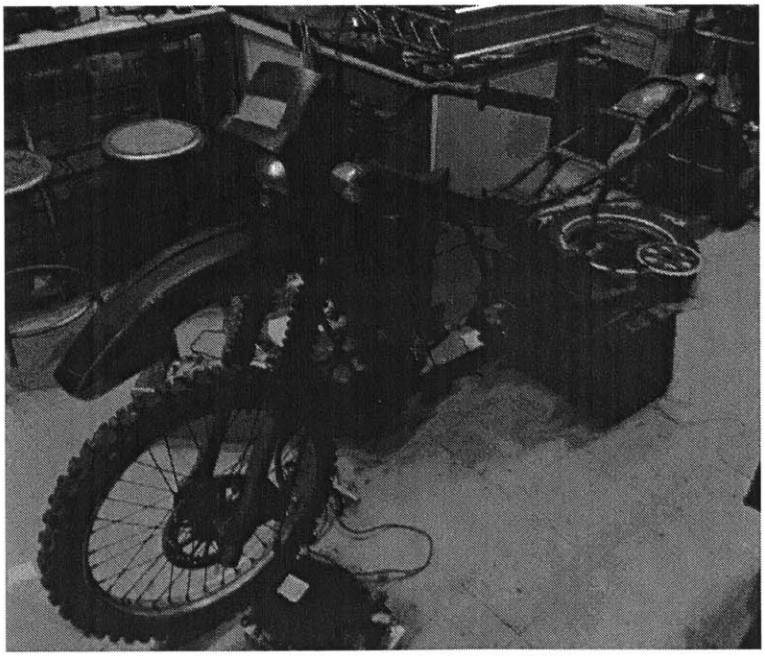

Figure 53: Donated XT-350

With both a vehicle and powertrain, work progressed quickly. Within one week, the vehicle rolled under its own power.

Figure 54: Motor and inverter attached to frame

My colleague designed a new interface board with more robust connectors.

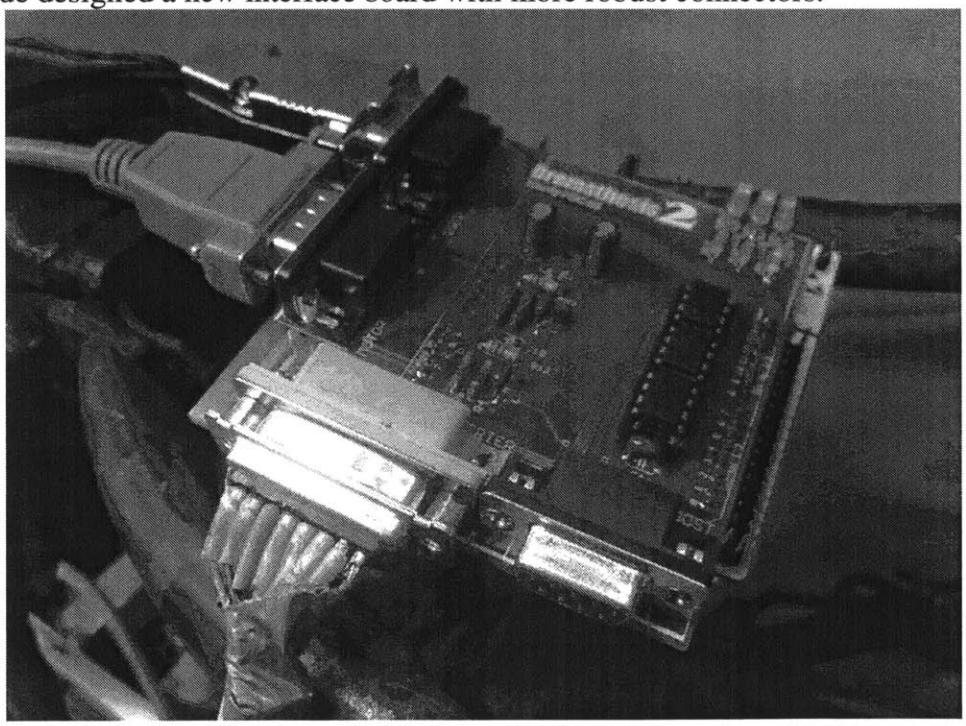

Figure 55: New interface board with DB style connectors

Effort was poured into making the vehicle safe to operate. The deteriorating wiring harness was remade, a killswitch and contactor were installed, and the brakes were serviced.

Figure 56: Box containing contactor, fuse, and a precharge circuit

Further data was collected to diagnose a stalling issue. It was eventually determined that the issue was caused by tripping an overcurrent condition on the inverter. The inverter shuts down and floats the phases when overcurrent is detected. The controller was naïve to this, and continued to command high current, rapidly getting the inverter to shut down again soon after turning on. Two changes were made in response to this. The inputs to the current loop were more heavily filtered to damp spurious readings, and the gearing of the vehicle was reduced after an error in a no-load speed calculation was found. More data was logged and the following graph was produced:

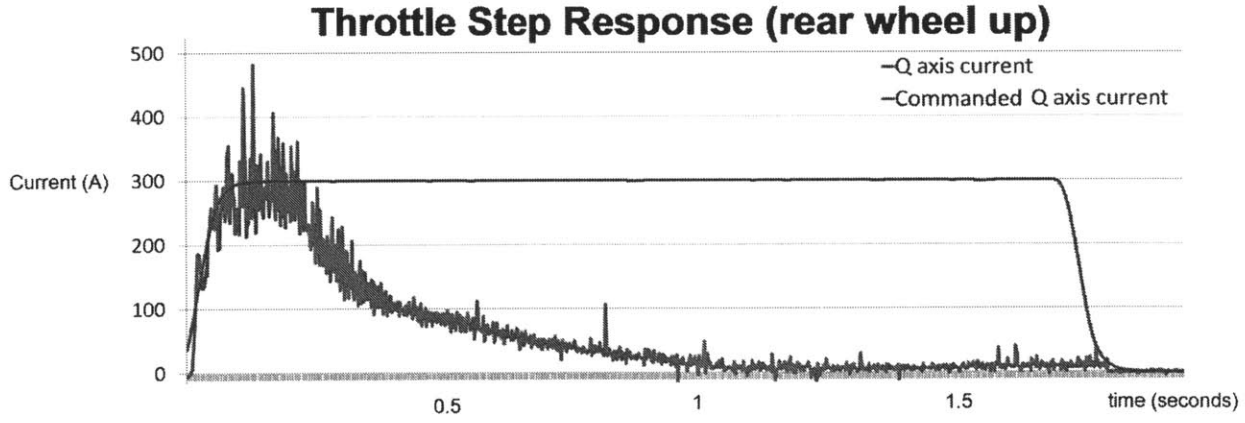

Figure 57: Plot of Q axis current vs time. The system starts at rest and receives a step in throttle. The current limit is set at 300A.

Although some current readings exceed the shutdown threshold of 400A, the inverter did not shut down due to overcurrent or otherwise during this test. Q axis current follows the command closely until the increasing back EMF of the motor begins to oppose the output of the inverter at around 0.2 seconds.

Conclusion

Used hybrid car parts consisting of MG1 from a Mercury Milan hybrid and the inverter from a 2nd generation Toyota Prius were combined with a custom controller performing field oriented control to form a functioning electric powertrain. The powertrain was attached to a dirt bike frame for load testing. This undergraduate thesis is complete, but the project is only just beginning[12].

Acknowledgements

Thanks to my friend and collaborator Bayley Wang for his expertise in electronics and programming, Mars for donating a dirtbike sans engine, Dane Kouttron for his enthusiasm and deep understanding of lithium batteries, the people of MITERS for technical help, love, and encouragement, and Professor Kirtley for advising this project and sharing his great knowledge of electric machines

Bibliography

[1] *http://www.hybridcars.com/news/december-20, "Cumulative US HEV Sales by year 1999 2009" by Mariordo (Mario Roberto Durán Ortiz) - Own work using data from http://www.afdc.energy.gov/afdc/data/vehicles.html (US DoE).Data for 2011 taken from HybridCars.com.*

[2] MIT Electric Vehicle Team, "Vehicle: elEVen," [Online]. Available: http://web.mit.edu/evt/nextvehicle.html.

[3] J. R. MEVEY, "SENSORLESS FIELD ORIENTED CONTROL OF BRUSHLESS PERMANENT MAGNET SYNCHRONOUS MOTORS," 2009.

[12] Further progress will be documented at http://nkirkby.scripts.mit.edu/nk/